Cryogenic spray quenching of a simulated propellant storage tank wall with heat transfer enhancement by a thin-film coating and flow pulsing in microgravity

J. N. Chung[1*], Jun Dong[1], Hao Wang[1], S. R. Darr[1], J.W. Hartwig[2]

1. Cryogenics Heat Transfer Laboratory

Department of Mechanical and Aerospace Engineering

University of Florida, Gainesville, FL, 32611-6300, U.S.A.

2. *NASA Glenn Research Center, Cleveland, OH, 44135, USA*

*Corresponding author. Tel.: 352-392-9607; fax: 352-392-1071

E-mail address: jnchung@ufl.edu (J. N. Chung).

Abstract

Human space exploration to the Moon, Mars, and possibly asteroids is NASA's biggest challenge for the new millennium. One of the critical elements to this mission is the effective, sufficient, and reliable supply of cryogenic propellant fluids. Future lower-earth-orbiting (LEO) propellant fuel depots and human-carrying orbital transfer spacecraft flying to the moon and Mars will have to utilize the high thrust and high efficiency of liquid cryogenic chemical propulsion or nuclear thermal propulsion. Efficient in-space tank-to-tank propellant transfer (propellant fuel depot to orbital transfer spacecraft) of cryogenic propellants is an enabling technology for the planned Crewed Mars Surface Mission. The transfer of cryogenic propellants in space, however, has yet to be accomplished, solely due to the unavailability of cryogenic quenching heat transfer data during chilldown (quenching) and filling of the propellant receiver tank in reduced gravity and microgravity as liquid propellant cannot be stored in a required liquid state until the tank is quenched down to the liquid temperature.

Therefore, highly energy efficient thermal-fluid management breakthrough concepts to conserve and minimize the cryogen consumption during propellant transfer have become the focus of research and engineering development, especially for the deep-space mission to Mars. In this paper, we introduce such concepts and demonstrate their feasibility for cryogenic storage tank chilldown in parabolic flights under a simulated space microgravity condition. In order to maximize the storage tank chilldown efficiency for the least amount of cryogen consumption, the technology adopted included cryogenic spray cooling, Teflon thin-film coating of the simulated tank surface, and spray flow pulsing. The completed flight experiments successfully demonstrated that spray cooling is the most efficient cooling method for the tank chilldown in microgravity. In microgravity, Teflon coating alone can improve the efficiency up to 72% and the efficiency can be improved up to 59% by flow pulsing alone. However, Teflon coating together with flow pulsing was found to substantially enhance the chilldown efficiency in microgravity for up to 113%.

INTRODUCTION

Importance of quenching heat transfer

The human space exploration from a low earth orbit to a high earth orbit, then to Moon, Mars, and possibly asteroids and moons of other planets is the biggest challenges for scientists and engineers for the new millennium. An indispensable part to this is the effective, affordable, and reliable supply of cryogenic fluids, and their thermal management in space. The efficient and safe utilization of cryogenic fluids in thermal management, power and propulsion, and life support systems of a spacecraft during space missions involves the transport, handling, and storage of these fluids in terrestrial, reduced gravity and microgravity conditions.

Lower-earth-orbiting (LEO) propellant fuel depots planned for future deep-space missions and human-carrying orbital transfer spacecraft flying to the moon and Mars will have to utilize the high thrust and high efficiency of liquid cryogenic chemical propulsion or nuclear thermal propulsion[1-4]. Efficient in-space tank-to-tank propellant transfer (propellant fuel depot to orbital transfer spacecraft) of cryogenic propellants is an enabling technology for the planned DRM 9 Crewed Mars Surface Mission[1]. The transfer of cryogenic propellants in space, however, has yet to be accomplished, solely due to the unavailability of cryogenic quenching heat transfer data during chilldown (quenching) and filling of the propellant receiver tank in reduced gravity and microgravity[4] as liquid propellant cannot be stored in a liquid state until the tank is quenched down to the liquid temperature. The consumed propellant during chilldown is a mixture of vapor and liquid that cannot be used for any purpose and therefore must be vented overboard. Since the current terrestrial chilldown technology can only manage to offer relatively very low thermal energy efficiencies[5] and further that it has never been developed under space microgravity conditions, a new break-through technology advance that significantly raises the chilldown efficiencies, and is also verified under space conditions is needed for enabling deep space missions.

In order to maximize the storage tank chilldown efficiency, the technology proposed includes cryogenic spray cooling, Teflon thin-film coating of the tank inner surface, and spray flow pulsing. The completed flight experiments successfully demonstrated that cryogen spray cooling is the most efficient cooling method for the tank wall chilldown in microgravity. Teflon coating together with flow pulsing was found to substantially enhance the chilldown efficiency in microgravity. The feasibilities of charge-hold-vent for tank chilldown and no-vent-fill for tank filling in microgravity were also successfully demonstrated.

According to publications by the members of the Space Cryogenic Thermal Management Group at NASA Glenn Research Center, Doherty et al.[6] and Myer et al.[7] provided the main areas of Research and Development for space cryogenic thermal management. In-space tank-to-tank transfer thermal management is composed of three operational elements – 1) high efficiency line chilldown 2) high efficiency tank chilldown 3) and no-vent fill of the receiver tank. When transferring a cryogenic propellant from a supply tank to a receiver tank, the transfer line (i.e. pipe and valves) and receiver tank are at high temperatures compared to that of the propellant. Chilldown is the process of introducing the cryogen into the system to cool the hardware down to the liquid temperature. The figure below shows the transient wall temperature (left) and heat flux (right) for chilldown of a pipe at a certain downstream axial location. The flowing propellant boils off as it cools the line and tank. Since the propellant is only storable and useful to the engine in pure liquid form, this vaporized propellant is vented overboard and considered "lost". Since each of the three elements is a two-phase flow process, they are all highly influenced by the gravity level. Among all three areas, receiver tank chilldown is considered the most important area as the amount of cryogen consumed is the largest. In this paper, we report an advance in microgravity tank wall chilldown heat transfer using a thin-film coating and spray cooling.

Characteristics of quenching heat transfer

A quenching (chilldown) process is a liquid-to-vapor phase change phenomenon that is governed by the "boiling curve". This curve[8] as shown in Fig. 1 illustrates the heat transfer surface heat flux, q'', plotted against the surface degree of superheating, $T_W - T_{sat}$, where T_W is the surface temperature and T_{sat} is the saturation temperature corresponding to the boiling fluid bulk pressure. In boiling, if the heating source is externally supplied to the heater surface such as the embedded electrical resistance heating element, the process is heat-flux controlled and it follows the route of A→B→D. In contrast, during quenching the warm wall where the heat transfers out does not have a source of heat supply, therefore, the heat transferring out of the wall can only come internally from the thermal capacity (stored energy) of the wall. The only way to remove heat from the wall is by lowering the inner wall surface temperature using a cooling flow. So quenching is a wall surface temperature-controlled process. Thus, a quenching process follows the route D→C→B→A. During quenching, film boiling is always the first mode of heat transfer encountered due to a relatively very hot surface. Owing to its relatively low heat fluxes at high wall temperatures, film boiling usually dominates the quenching time and cannot be avoided. As a result, in traditional quenching processes, the thermal energy efficiency is extremely low. According to Shaeffer et al.[5] , the average quenching efficiency that is defined as the ratio of the amount of thermal energy removed from the wall versus the required cooling capability of the cryogen spent in a quenching process is about 8%, highlighting the tremendous need to improve the quenching efficiency for many applications that require cryogens as the working fluid.

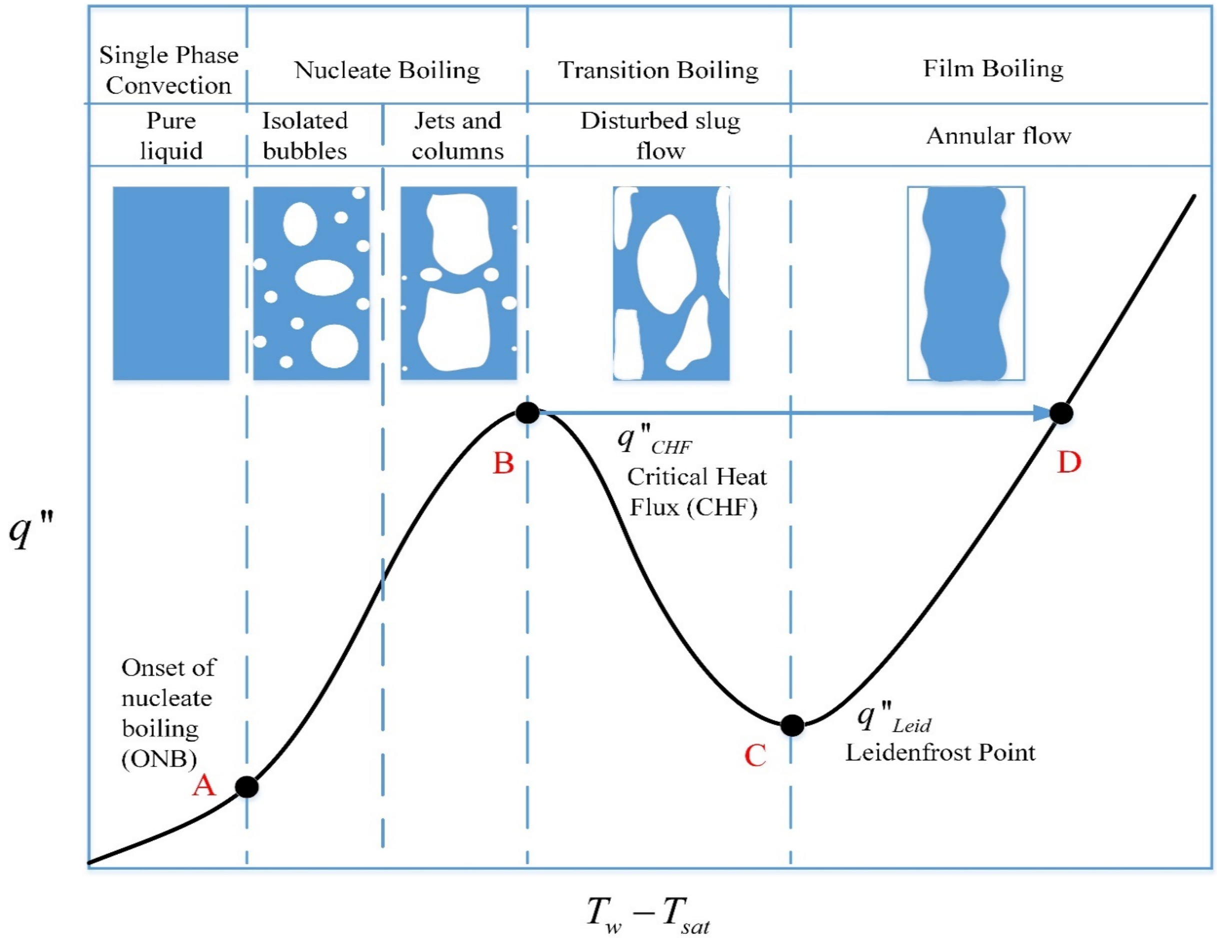

Fig. 1. A typical boiling curve including different boiling regimes and corresponding flow patterns.

Literature review

Spray cooling

Progressive advances in high power density electronics, and high-performance energy systems have precipitated the need for innovative thermal management technologies to ensure reliable performance and reduce the payload of thermal management systems. Such systems include high current density propulsion systems, high power electronics for energy conversion, high power optical sensors, as well as high power microelectronics packaged within environmental enclosures. In order to manage the progressively increasing heat flux requirements for thermal management systems, spray cooling system has been proposed and under constant development for the past sixty years. Liang and Mudawar[9] indicated that spray cooling possesses several advantages: high flux heat dissipation, low and fairly uniform surface temperature, and ability to cool are relatively large surface area using a single nozzle.

In very recent papers, Liang and Mudawar[9,10] provided a highly comprehensive, thorough and complete review of the spray cooling research up to 2017. Almost all of the published papers were using water and refrigerants and we found only three papers on the study of terrestrial cryogenic spray cooling. Sehmbey et al.[11] performed liquid nitrogen spray cooling experiment to gather heat transfer characteristics to facilitate the operation of power electronics at very low temperatures. Four different nozzles at various pressures were used to study the variation in spray cooling heat transfer at liquid nitrogen temperature. The effect of nozzle and flow rate on the critical heat flux and overall heat transfer characteristics were presented. Cooling heat fluxes close to 1.7 x 10^6 W/m^2 were realized at temperatures below 100 K. The mass flow rate range was from 6.1 x 10^4 kg/h m^2 to 3.2 x 10^5 kg/h m^2. They demonstrated that a high heat flux (over 1.0 x 10^6 W/m^2) cooling technique, such as spray cooling, will have to be used to realize all the advantages of low-temperature operation. Followed their experimental study, Sehmbey et al.[12] further provided empirical correlations for liquid nitrogen spray cooling. They offered a general semiempirical correlation (based on macrolayer dryout model) for spray cooling critical heat flux (CHF) for different liquids and spray conditions. An empirical correlation for heat flux was also presented. They also pointed out the importance of surface roughness for spray cooling with liquid nitrogen. It was discovered that the rougher surfaces have significantly higher heat transfer rates and similar CHFs occurring at lower temperatures.

Somasundara and Tay[13] investigated the intermittent liquid nitrogen spray cooling for applications which require higher heater operating temperature (-180 C to 20 C). This intermittent spray cooling process can be adjusted using the mass flow rate, pulsing frequency and duty cycle (percentage of open time in one cycle) to match the required cooling rate on the target. The intermittent spray experiments were conducted for various ranges of surface temperatures.

Kato et al.[14] studied the gravity effects on liquid spray cooling using a nickel-plated copper block in terrestrial and variable gravity conditions on board parabolic flight. The copper block was first heated by seven cartridge heaters to a prescribed temperature and then cooled down by spraying water or CFC-113 onto the nickel-plated surface which is only 19 mm in diameter. They observed that the heat transfer in the low heat flux regime below the CHF was enhanced by the reduction in gravity for both fluids. However, the effects of reduced gravity act differently on these two fluids at CHF. The CHF for CFC-113 was decreased in a low gravity level whereas the CHF of water increased. Kato et al.[14] also reported the vanishing of the gravity effect on the heat transfer at high spray volume mass fluxes.

As a follow-up study, Yoshida et al.[15] conducted a more comprehensive study of the effects of gravity on spray cooling. Two different heaters were used in this study. One is similar to the copper block described by Kato et al.[14] except that the surface was plated with chromium and 50 mm in diameter. The other was a glass prism plated with a thin transparent indium tin oxide (ITO) film as the heating element. This transparent glass heater was used in order to visualize the liquid deposition on the heater surface for steady state spray cooling while a copper block was used for transient spray cooling test. The working fluids used were water and FC-72. A series of ground-based tests and parabolic flight tests were performed by varying the test parameters such as working fluid, heater surface orientation, heat flux at heater surface, mass flux of the coolant as well as heater types. They reported that gravity level had little effect in the nucleate boiling regime. Moreover, they suggested a coupled effect of gravity and spray volume mass flux on CHF. In the case of a low spray volume flux, neither the magnitude nor the direction of gravity affected CHF.

However, the CHF under reduced gravity is higher than that under the hyper gravity by 10 percent. They also noted the significant influence of gravity on the film boiling regime when the Webber number was low. And they argued that the deterioration of the heat transfer during the film boiling in the case of low Webber number and reduced gravity condition is due to a lack of secondary impingement on the heater surface.

As indicated by the literature review above, we only found a handful of terrestrial cryogenic spray cooling research papers. However, there has been no attempt on the microgravity and reduced gravity cryogenic spray cooling using either room-temperature liquids or cryogens. We believe that the current paper is the first to report the experimental data on cryogenic spray cooling in reduced gravity.

Pulsed flow enhancement

According to transient conduction heat transfer[16] when we place two materials A and B, each with a different temperature in contact, the transient heat fluxes $q''_{A\to B}$ across the interface from A to B is given by Eqn. (1).

$$q''_{A\to B} = \frac{k_A(T_{A,i} - T_s)}{(\pi\alpha_A t)^{1/2}} = -\frac{k_B(T_{B,i} - T_s)}{(\pi\alpha_B t)^{1/2}} \quad (1)$$

Where k_A and k_B are thermal conductivities of A and B, respectively. $T_{A,i}$ and $T_{B,i}$ are initial temperatures of A and B before contact, respectively. α_A and α_B are thermal diffusivities of A and B, respectively. T_s and t are the common interface temperature and elapsed time, respectively.

$q''_{A\to B}$ would be proportional to $t^{-1/2}$ (since t is the elapsed time after the initial contact of the two materials, so $t=0^+$ is the time when the two are placed in contact) as the rest of the parameters (thermal properties) in the equation are all constants. The physical meaning is that initially the heat transfer would be very high and the heat flux decreases quickly as time passes. As a result, for the pulsed flow quenching process, every time when the pulsed flow is turned on after the off period in a duty cycle the test surface gets in contact with a fresh cooling fluid that causes a corresponding spike in the heat transfer flux that results in higher heat transfer than the continuous flow case. Chung et al.[17] found that the pulsed flow would raise the chilldown efficiency up to 67% over the continuous flow case for the convective chilldown of a pipe.

Low-thermal conductivity coating

The enhancement concept of coated tube is based on that there are two heat transfer mechanisms involved that are opposite in nature to each other. The first mechanism is the thermal insulating effect due to the low-thermal conductivity thin layer that facilities a fast drop of the tube inner surface temperature by restricting the heat flow from the bulk of the tube wall to the tube inner surface. The lower surface temperature allows the quenching process to quickly move from film boiling regime to the Leidenfrost point to initiate the higher heat transfer transition and nucleate boiling regimes. The second mechanism is the conduction of heat from the bulk of the tube wall to the cooling fluid through the inner surface during transition and nucleate boiling regimes that requires the thermal conductivity of the bulk wall material to be as high as possible such as metals to expedite the wall cooling process. There should exist an optimal thickness of the low-thermal conductivity layer that balances these two competing mechanisms such that the coating is just thick enough to quickly lower the tube surface temperature to that of the Leidenfrost point while it is still relatively very thin to not substantially reduce the heat flow from the bulk to the cooling fluid. Chung et al.[18,19] used thin-layers of Teflon for enhancing heat transfer during chilldown of a metal pipe and they found that the coatings could increase the chilldown heat transfer efficiency up to 109% and 176% in terrestrial gravity[18] and microgravity[19], respectively.

Research objective

The primary objective of the current set of microgravity experiments is to obtain transient quenching heat transfer characteristics of a typical storage tank wall surface simulated by a metal circular disk. The disk transient temperature history or a chilldown curve during spray quenching from room temperature to LN2 saturation temperatures was measured. One of the two disks was coated with a low thermal conductivity thin Teflon layer to evaluate the heat transfer enhancement. The effectiveness of the coating was evaluated by a comparison of chilldown efficiencies with coating to those of a bare surface disk. Tests were carried out with a set of pulse flow conditions that includes 40%, 50%, and 70% duty cycles with 1 second period over a wide range of test section inlet pressure levels and corresponding mass flow rates. The effectiveness of the pulse flow was evaluated by a comparison of chilldown curves with flow pulsations to those with constant and continuous flows.

RESULTS

Microgravity experiments completed

The University of Florida flight team led by Professor Jacob Chung performed parabolic flight experiments in one flight on 12 November 2018. Since we only had one parabolic flight to perform the experiments, we were only able to use one test section configuration. As shown in Fig. 14, the test section is composed of two disks facing each other and they were sprayed on by two separate spray nozzles, respectively, sharing the same liquid nitrogen feed line such that we could obtain two sets of chilldown data with identical spray flow condition simultaneously in one experimental run. As discussed in the Method section, one target was a stainless-steel disk coated with a low-thermal conductivity Teflon 959G-203 thin-film layer[22], and the other was the bare surface stainless steel disk without any coating to serve as the baseline case for evaluating the coating effects. Table 1 lists the six cases we performed during the one parabolic flight experiment. It is noted that the gravitational acceleration for Mars is 3.711 m/s^2 that is 37.8% of earth gravity of 9.81 m/s^2. In our notation, the Martian gravity is 0.378g where g is earth gravity. As mentioned above, the gravity under simulated microgravity environment in the parabolic flight is about ±0.01g.

Table 1. Test conditions for the 8 cases.

Case	P_{in} (psig)	Duty Cycle (%)	Period (second)	g-level
1	80	100	NA	microgravity
2	80	40	1	microgravity

3	80	70	1	microgravity
4	60	100	NA	microgravity
5	90	100	NA	microgravity
6	90	50	1	microgravity

Typical chilldown curves

As shown in Fig. 2, for measuring the disk transient temperature variation history during the chilldown for determining the quenching efficiency, 25 thermocouples (TCs) were soldered to the vacuum side (back) of the test disk. A total of 23 TCs are distributed on 6 concentric circles (6 rings, R1,R2,…., R6) in addition to one (TC 25) placed at the center and one (TC 5) placed on the outside near the outer boundary. TC 5 is 3.7" away from the center of the disk plate.

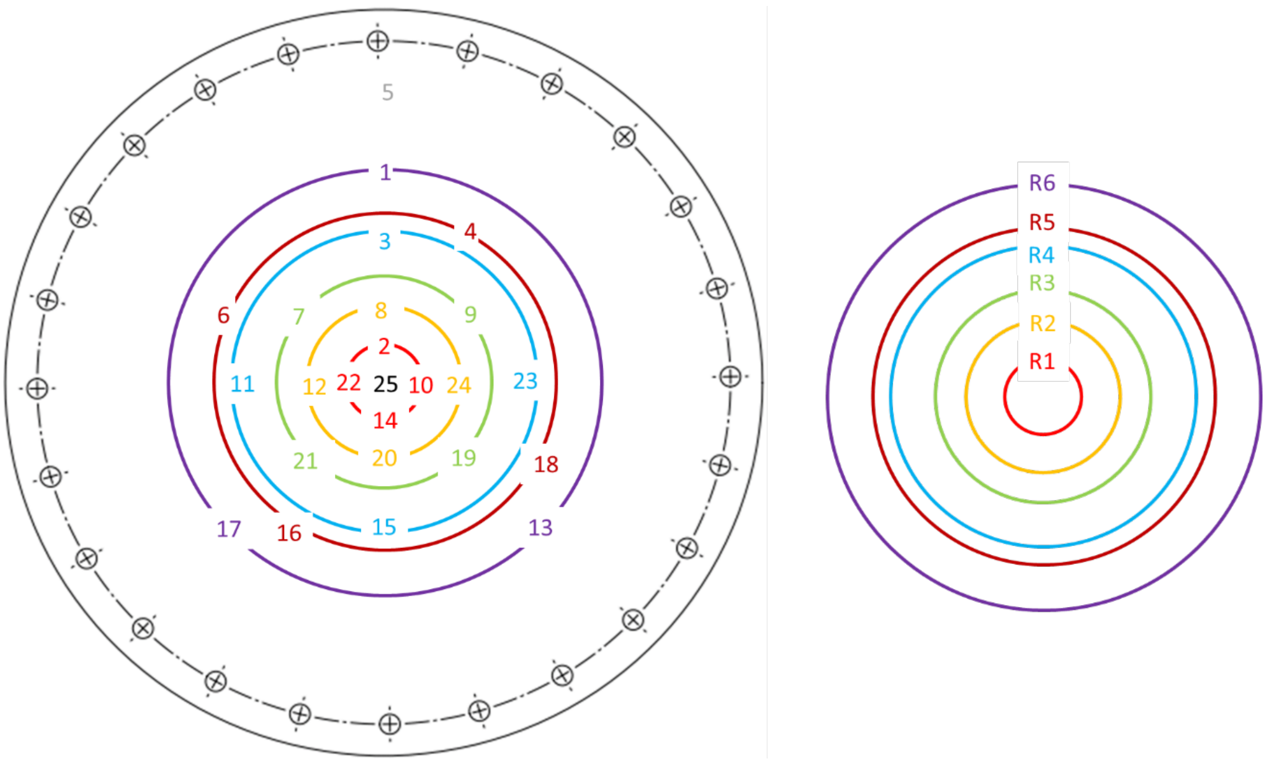

Fig. 2. Locations of 25 thermal couples.

A chilldown curve for a local point on the disk is defined as the transient temperature history at this point recorded by a thermal couple (TC) during the chilldown process. So, these curves are the plots of the temperatures measured by the TCs soldered on the back of the disk that registered the disk back local surface temperature histories during chilldown. Fig. 3(a) shows a typical set of full 25 chilldown curves from a spray quenching experiment. The chilldown curves shown in Fig. 3(a) were obtained from the bare surface stainless steel disk in 1-g conditon. Fig. 3(b) is a simplified version of Fig. 3(a) where only the medium chilldown curve for each ring is plotted in addition to the center TC 25 and outer boundary TC 5. A medium chilldown curve is the one with a chilldown time in the middle among those of the four curves from the same ring. At any instant, for a local point on the back surface is the warmest and the corresponding point on the front surface is the coolest, therefore, chilldown at a point is considered complete only when the back temperature at that point has reached the saturated liquid temperature corresponding to the local pressure. Chilldown time is therefore defined based on the disk back surface temperatures. As seen in Fig. 3(a), based on the individual TC's distance from the center, we have divided the chilldown curves into four groups identified by red, green, yellow and purple double-headed arrows. The red group includes the center TC and all four TCs on R1, the green group includes all eight TCs on R2 and R3, the yellow group includes all eight TCs on R4 and R5, and the purple group includes three TCs on R6. The color is also used to identify the TCs as shown in Fig. 2. For example, TCs 2, 10, 14, 22 and 25 belong to the red group. As a result, the red group is closest to the center, the green group is the next closest, the yellow group is next closest to the green group, and the purple group is the farthest. It is very clear that the closer to the center the faster the rate of chilldown. The center (TC 25) is always the fastest chilldown point. As a result, all the chilldown curves are aligned in a predictable order which is that the chilldown curve from a TC that is located farther from the center is always positioned to the right side of the curve from a TC located closer to the center.

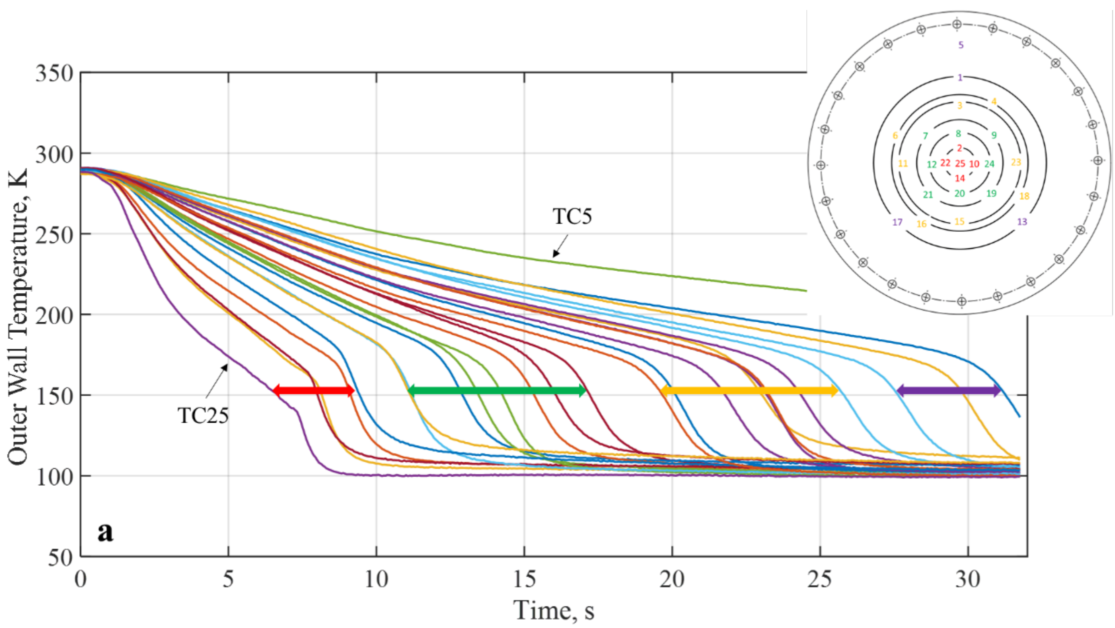

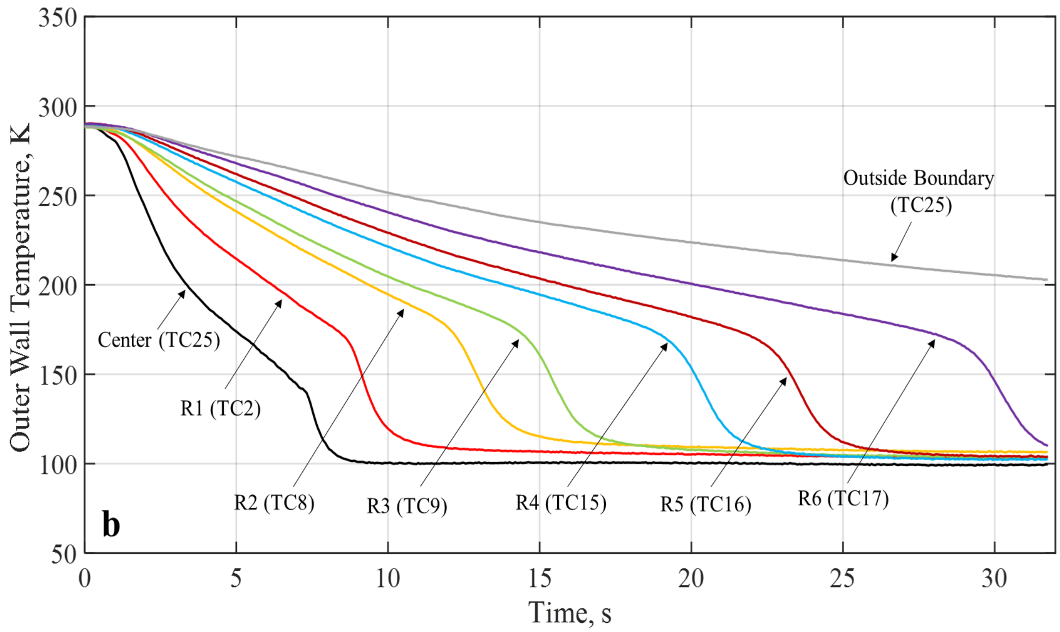

Fig. 3. Typical chilldown curves. (a) A typical set of full 25 chilldown curves from a bare surface stainless steel disk spray chilldown experiment, (b) a simplified set of chilldown curves from Fig. 3a.

Boiling curves

For every chilldown curve, there exists a corresponding unique boing curve. A boiling curve illustrates the heat transfer characteristics during chilldown by providing the inner wall transient surface heat flux as a function of inner wall surface temperature. Figs. 4(a) and 4(b) provide two sets of chilldown curve versus boiling curve plots with data obtained by the center TC25 and TC9 on Ring 3, respectively, for Case 1 using the bare surface disk. It is noted that the tube inner surface temperature and heat flux were obtained using the measured outer wall surface temperature through an inverse conduction method developed by Burgraff[20]. Readers are referred to current authors' previous papers[17,18] for details. The chilldown curve and corresponding boiling curve as shown in Fig. 4 share the common inner surface temperature scale. As explained in Fig. 1, the boiling curve shows the heat transfer regimes, Leidenfrost point (LFP) and CHF point as a function of the inner surface temperature. As indicated in Fig. 4(b), film boiling takes place from the start to the LFP, followed by transition boiling between the LFP and the CHF point. Nucleate boiling ensues after the CHF point. As also can be seen in Fig. 4(b), for LN2 chilldown, the majority of time is spent in the film boiling regime. After the rewetting (LFP), the heat fluxes are much higher in the transition boiling regime and nucleate boiling regime that results in the rapid cooling of the tube wall and a corresponding sudden increase in the slope of the chilldown curve. As shown in Fig. 4(a), the LFP is located just ahead of the slope change of the chilldown curve, and the almost vertical line corresponds to the transition and nucleate boiling regimes with the CHF separating the two regimes.

For the Fig. 4(a) center TC25 case, the film boiling regime lasted 7.3 s. The transition and nucleate boiling together lasted about 0.5s–1s, after which single-phase liquid convection heat transfer followed at very low heat fluxes. The main reason for this elapsed time difference is that the film boiling heat fluxes are lower than those in transitional and nucleate boiling. It is also noted that the rewetting (LFP) temperature, T_{wet}, is 145K. Comparing between Figs. 4(a) and 4(b), the heat transfer rates at the center were much higher than those at TC9 location due to higher spray mass fluxes at the disk center that resulted in much quicker chilldown time at the center.

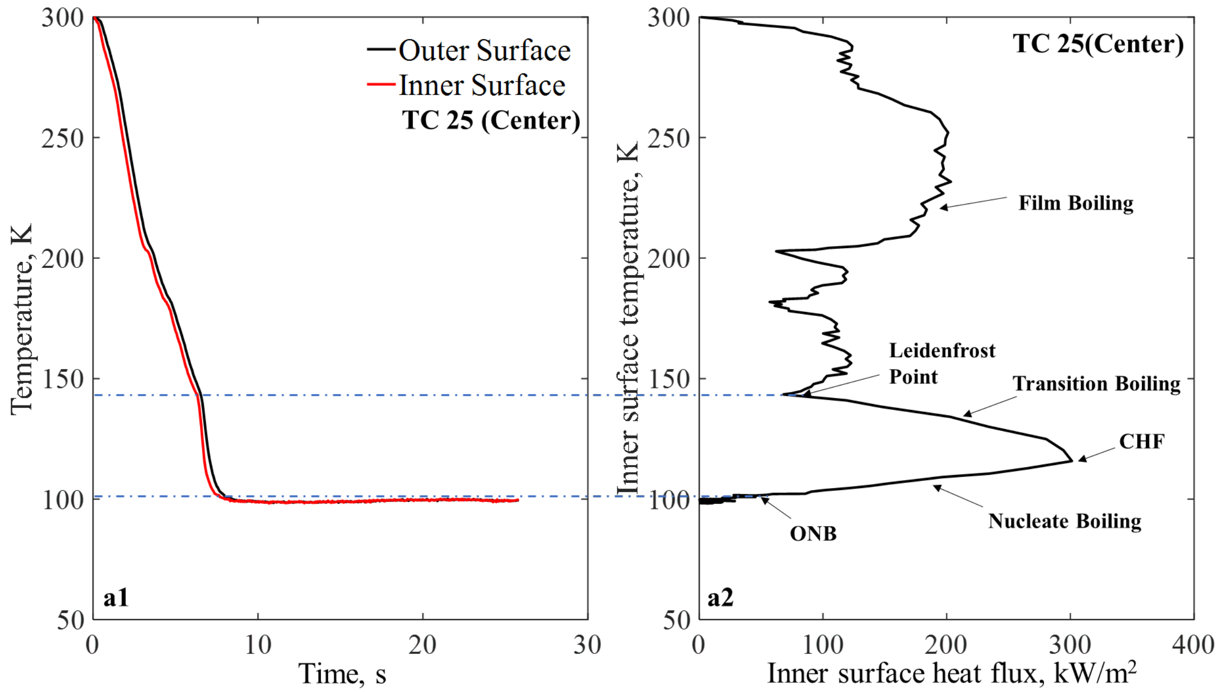

(a)

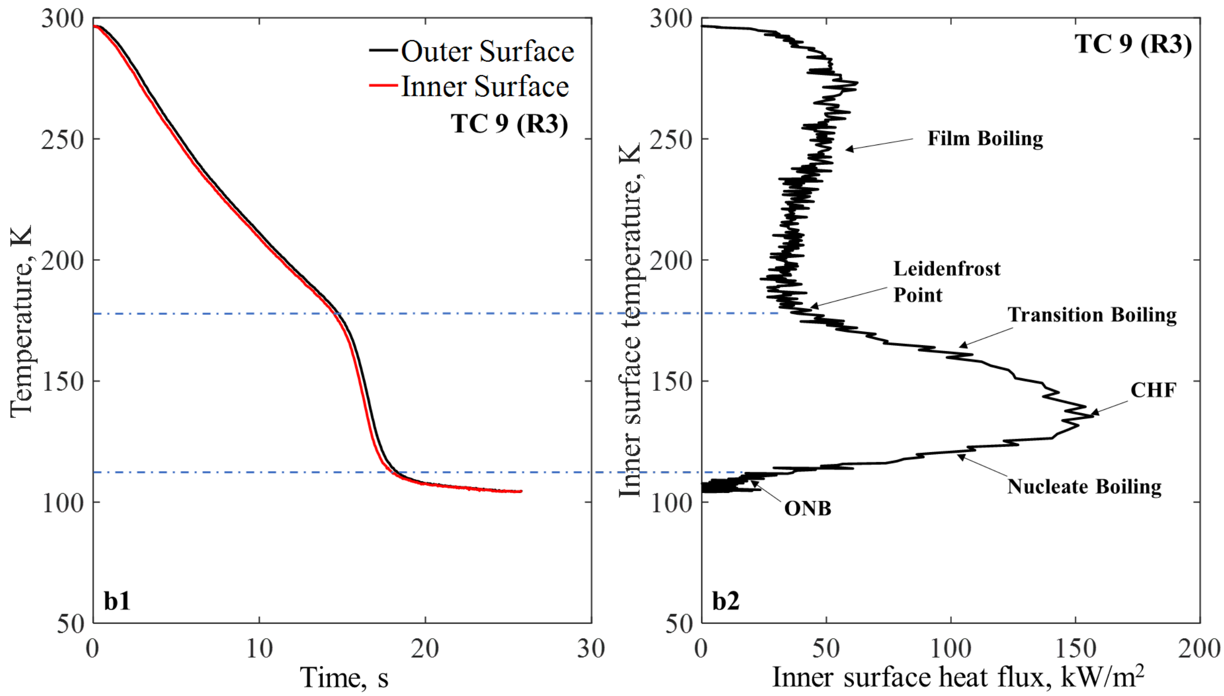

(b)

Fig. 4. Chilldown curve and Boiling curves for Case 1, 80 psig inlet pressure, and continuous flow with stainless steel bare surface disk in micro-G, (a1) chilldown curve from center TC, (a2) boiling curve from center TC, (b1) chilldown curve from TC9 on Ring 3, and (b2) boiling curve from TC9 on Ring 3.

Disk plate chilldown thermal efficiencies

In order to measure the spray chilldow performance, we adopted a spray thermal efficiency concept that measures how much of the cooling capacity of the supplied spray cryogenic liquid is actually utilized in chilling down the disk. The chilldown efficiency as defined below represents the percent of available total quenching capacity of the liquid cryogen supplied that is actually utilized in cooling the disk (target of spray cooling) from room temperature to liquid saturation temperature of LN2 corresponding to spray chamber pressure. The spray chilldown thermal efficiency for a disk plate, η_{CD}, is therefore defined as,

$$\eta_{CD} = \frac{Q_{\mathrm{Removed}}}{Q_{Available}} \times 100\% \quad (1)$$

In the above, Q_{Removed} is the total thermal energy removed from the disk plate by the cooling fluid during chilldown and is defined as,

$$Q_{\text{Removed}} = \left(M_{\text{TARGET}}\right) c_{p,SS} \left(T_{initial} - T_{final}\right) + \left(M_{\text{NON-TARGET}}\right) c_{p,SS} \left(T_{initial} - T_{NON-TARGET,AVERAGE}\right) \quad (2)$$

where M_{TARGET} is the mass of the chilldown target area that totally intercepts the spray cone and completely cooled down by the spray fluid to the saturated liquid nitrogen temperature. It is noted that the target area is also a circular disk with a radius of r_{target} which is part of the whole disk with a radius of r_D from the center. $c_{P,SS}$ is the stainless steel specific heat for the disk plate material. $T_{Initial}$ and T_{Final} are the initial temperature when the chilldown is started and the final temperature of the target when the chilldown is completed, respectively. The end of chilldown temperature is the liquid saturation temperature corresponding to the local pressure. $M_{\text{NON-TARGET}}$ is the non-target area that does not receive any liquid spray and is therefore equal to the total disk plate mass, $M_{DISK\ PLATE}$ minus that of the target area, $M_{\text{NON-TARGET}} = M_{\text{DISK PLATE}} - M_{\text{TARGET}}$. $T_{\text{NON-TARGET, AVE}}$ is the estimated mass averaged temperature of the non-target area at the end of chilldown based on the conservation of thermal energy. $T_{\text{NON-TARGET, AVE}}$ is calculated using the flowing equation,

$$\left(M_{\text{NON-TARGET}}\right) c_{p,SS} \left(T_{initial} - T_{NON-TARGET,AVERAGE}\right) = Q_{\text{NON-TARGET}} \quad (3)$$

$$Q_{\text{NON-TARGET}} = \int_0^{t_{end}} q''_{Boundary\ of\ \text{Target}}(t) 2\pi r_{\text{Target}} t_{Plate} dt \quad (4)$$

Where $q''_{Boundary\ of\ \text{Target}}(t)$ *is time dependent heat flux due to heat conduction at the* interface between the target and non-target areas. The non-target area is only cooled by conduction heat flow through the interface betweenas the target and non-target areas as the non-target surface area does not receive spray droplets for cooling. r_{Target} is the radius of the target area and t_{plate} *is* the thickness of the disk plate. $q''_{Boundary\ of\ \text{Target}}(t)$ can be estimated by using the commercial software, Ansys Fluent, with the two measured chilldown curves as the boundary conditions. One chilldown curve at the outer boundary of target area and the other at the outer boundary of the non-target area were used *as the boundary conditions*.

$Q_{Available}$ is the total quenching capability supplied during the chilldown process. It is defined as,

$$Q_{Available} = M_{coolant} h_{fg} \tag{5}$$

Where $M_{Coolant}$ is the total mass of coolant used and it can be estimated as,

$$M_{Coolant} = \int_0^{t_{End}} \dot{m}(t)dt \tag{6}$$

$\dot{m}(t)$ is the recorded time-dependent coolant mass flow rate and t_{End} is the end of chilldown time that corresponds to the time when the entire target area has reached T_{Final}. Therefore, $M_{Coolant}$ is the total mass of cryogenic coolant consumed in the entire chilldown process. h_{fg} is the latent heat of vaporization per unit mass that means $Q_{Available}$ is the available total quenching capacity.

For cases where the target area is not totally chilled down during the microgravity period, use the following for $Q_{\text{Re}moved}$.

$$Q_{\text{Removed}} = \left(M_{TARGET\,sub1}\right)c_{p,SS}\left(T_{initial} - T_{final}\right) + \left(M_{TARGET\,sub2}\right)c_{p,SS}\left(T_{initial} - T_{AVE,TARGET\,sub2}\right) + \left(M_{\text{NON-TARGET}}\right)c_{p,SS}\left(T_{initial} - T_{NON-TARGET,AVERAGE}\right) \tag{7}$$

$M_{TARGET\,sub1} = mass\ of$ target subregion 1 where it is completely chilled down.

$M_{TARGET\,sub2} = mass\ of$ target subregion 2 where it is partially chilled down.

$T_{AVE,TARGET\,sub2} = average$ temperature of targert subregion 2 at the end of chilldown, t_{End}.

Uncertaity of chilldown efficiency

To find the uncertainty in chilldown thermal efficiency, η_{CD}, Eqs. (1) to (7) were cast in terms of seven independent quantities. The uncertainty of the chilldown efficiency was determined by applying the individual uncertainties of the seven quantities (listed in Table 2) using the root-mean-square method. The relative uncertainties for the coated disk and bare surface disk thermal efficiencies in microgravity range between 7.40% to 7.58% and between 8.71% to 9.44%, respectively.

Table 2. Individual uncertainty of the independently measure quantities

Symbol	Quantity	Measurement Method	Uncertainty
D	Diameter of the target area	Rulers	1.6×10^{-3} m
ρ	Density of test section	NIST website	1%
c_p	Specific heat capacity of test section	NIST website	5%
ΔT	Temperature difference between the initial and the end of the test	T-type thermocouple	1.5%
τ	Thickness of test section	Calipers	3×10^{-5} m
h_{fg}	Latent heat of nitrogen	NIST website	5%
$\dot{m}_l$	Mass flow rate of liquid nitrogen	Coriolis flow meter	0.3%

Table 3 lists the estimated chilldown efficiencies using Eqs. (1)-(7) for all six cases. For each case, there are four entries for microgravity gravity versus terrestrial gravity. Additionally, for each gravity condition, there are comparison between the bare surface stainless steel disk and the Teflon coated disk. For Cases 5 and 6, chilldown efficiencies for microgravity conditions were estimated based on incomplete mass flow rates and marked by an *. The actual complete mass flow rates were not available for microgravity conditions due to some intermittent lower flow rates that were below the measurement threshold of the Coriolis flow meter due to low liquid capacity in the supply tank during later stages of the parabolic flight experiment. Therefore, these two cases are somewhat between continuous flow and intermittent flow conditions. When the liquid capacity is lower than 50% in the tank, the pressure driven flow mechanism was not able to completely fill the entrance of the transfer pipe completely with liquid during microgravity that resulted in some mass flow rates that are lower than the flow meter measurement threshold.

With the six cases investigated, the efficiencies range between 19% - 29% and 13% - 21% for coated disk and bare surface disk in microgravity, respectively. However, in terrestrial gravity, the efficiency ranges are 17% - 29% and 14% - 22% for coated disk and bare surface disk, respectively. In general, the spray chilldown (cooling) efficiencies using cryogenic fluids are significantly higher than those using water or FC 72 that normally carry efficiencies only from 5% to up to about 10% [8.9].

Table 3. Chilldown efficiency

	Reduced-G		Ground -G	
Case	Teflon coated	Bare SS304	Teflon coated	SS304
1 (micro-g) 80 psig, continuous flow	18.54%	13.38%	23.19%	19.54%
2 (micro-g) 80 psig 40% DC, 1s Period	28.50%	21.26%	28.49%	21.74%
3 (micro-g) 80 psig 70% DC, 1s Period	23.48%	13.65%	21.17%	17.78%
4 (micro-g) 60 psig, continuous flow	28.40%	17.83%	24.50%	18.58%

5 (micro-g) 90 psig, continuous flow	16.87%*	12.96%*	17.26%	14.32%
6 (micro-g) 90 psig 50% DC, 1s Period	23.88%*	18.63%*	20.52%	16.76%

Microgravity chilldown curves

Fig. 5 presents the spray chilldown curves for Case 1 that has an inlet pressure of 80 psig and a continuous flow. Figs 5(a) and 5(b) are microgravity runs for coated and bare surface tubes, respectively. To provide a comparison, Figs. 5(c) and 5(d) are terrestrial counterparts for coated and bare surface tubes, respectively. The common feature for all four curves is that all curves show the typical quenching characteristics of a chilldown curve as discussed above. For both1-g and microgravity, the coated disk was chilled down much faster than bare surface disk. In microgravity, only the coated disk completed the chilldown within the 17-seond reduced gravity time. For example, as shown in Figs. 5(a) and 5(b) for Case 1 up to Ring 4, the coated disk was completely chilldown in 12.8 seconds, while the bare surface disk took 25 seconds. It is worth noting that under both 1-g and microgravity, for the coated tube, the chilldown curves of the center (TC25) and Ring 1 (TC2) do not exhibit the typical sequence of starting with film boiling. In other words, these curves do not have a distinct Leidenfrost point.

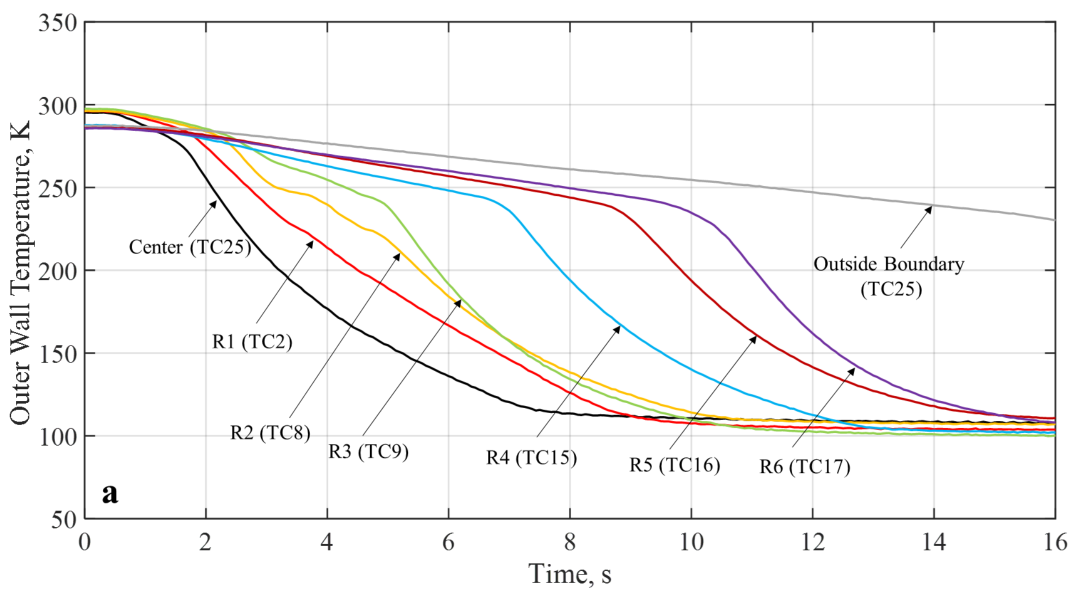

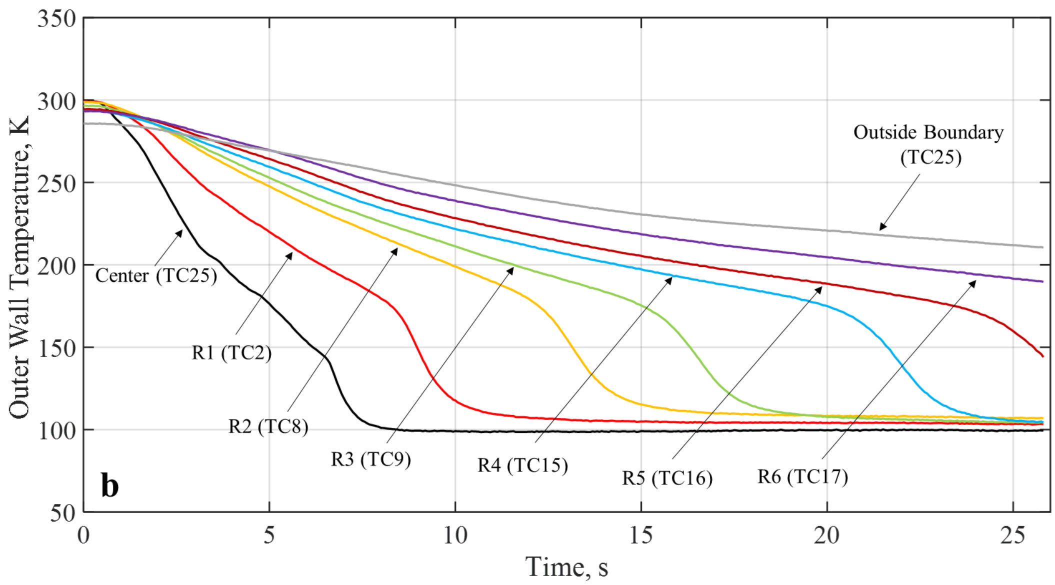
Outer Wall Temperature, K
Time, s
Outside Boundary (TC25)
Center (TC25)
R1 (TC2)
R2 (TC8)
R3 (TC9)
R4 (TC15)
R5 (TC16)
R6 (TC17)
b

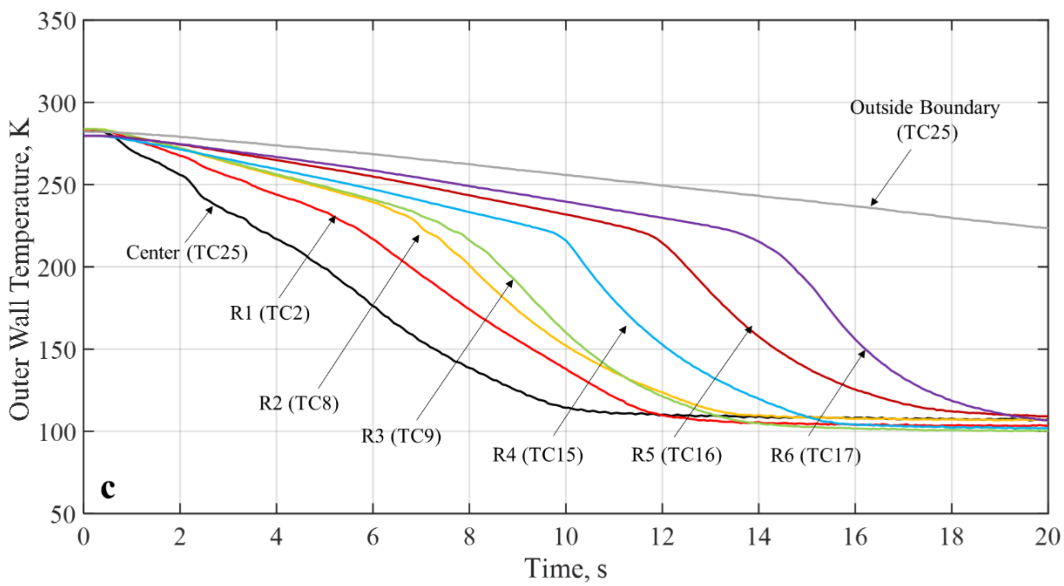
Outer Wall Temperature, K
Time, s
Outside Boundary (TC25)
Center (TC25)
R1 (TC2)
R2 (TC8)
R3 (TC9)
R4 (TC15)
R5 (TC16)
R6 (TC17)
c

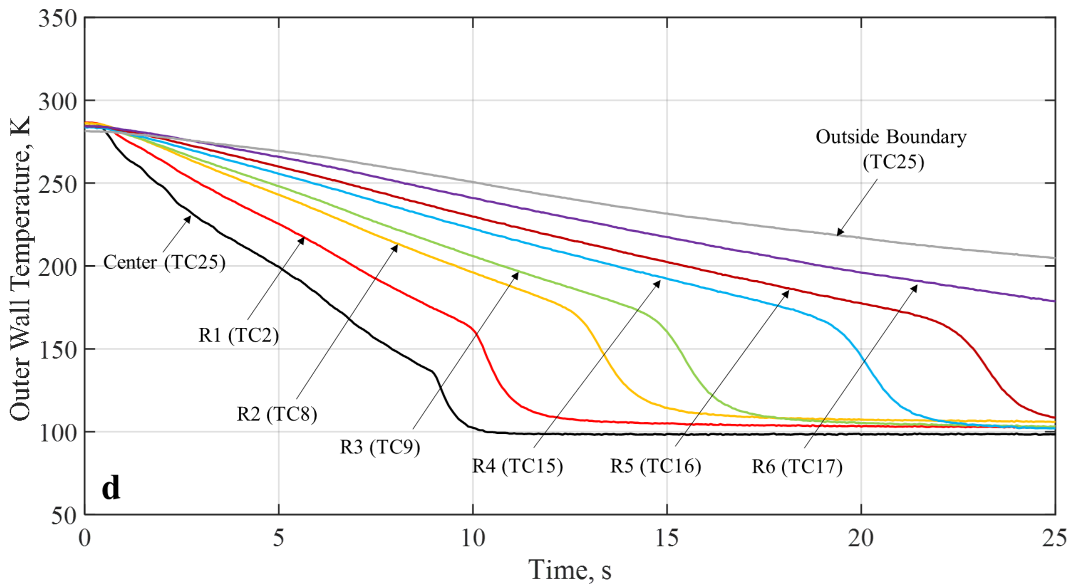

Fig. 5. Simplified chilldown curves for 80 psig inlet pressure, continuous flow (Case 1), (a) Teflon coated disk in micro-G (b) stainless steel bare surface disk in micro-G, (c) Teflon coated disk in terrestrial gravity, (d) stainless steel disk in terrestrial gravity.

Figs. 6-10 show the microgravity chilldown curves for the rest of five cases. For each case, there are two plots, one for the Teflon coated disk and the other for the bare surface stainless steel disk. It is noted that a complete chilldown up to Ring 6 within the 17-20 seconds of reduced gravity time was only feasible for the coated disks as the bare surface disk took much longer to reach to the same conditions. For example, specifically for Case 3 (Fig. 7(b)), Case 4 (Fig. 8(b)), and Case 6 (Fig. 10(b), even the center was not completely chilled down in 20 seconds. All the chilldown curves show the similar characteristics of spray quenching cooling where the local rate of cooling heat transfer is inversely proportional to the distance between the local point and the center of the disk. In general, for all cases the coating substantially expedited the chilldown process. For example, as shown in Fig. 11 for Case 2 up to Ring 4, the coated disk was completely chilldown in 12.8 seconds, while the bare surface disk took 25 seconds. More specifically, we will discuss quantitatively the enhancement of chilldown by the low-thermal conductivity coating below.

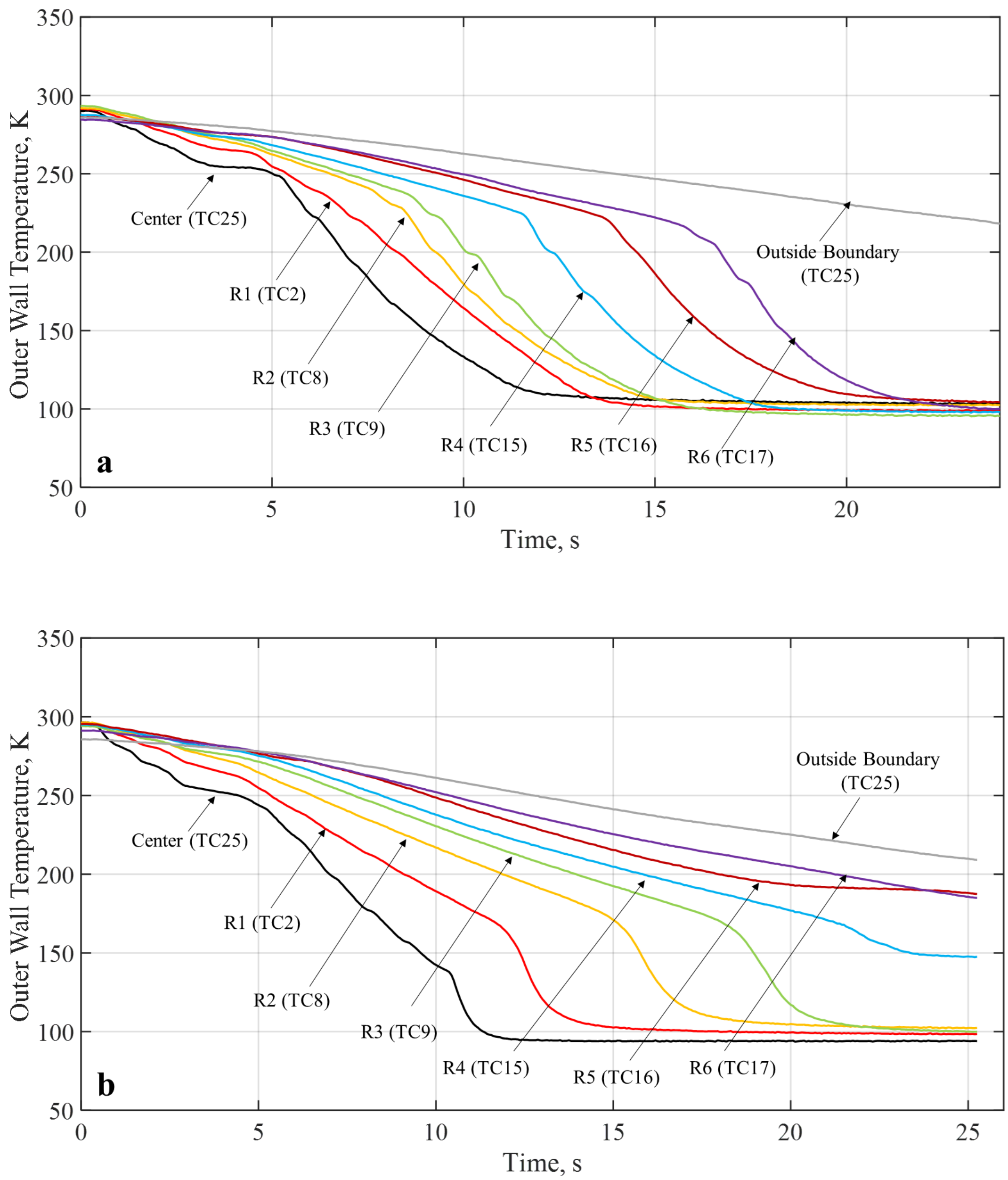

Fig. 6. Simplified chilldown curves for micro-G, 80 psig inlet pressure, 40% DC, 1s period (Case 2), (a) Teflon coated disk (b) stainless steel disk.

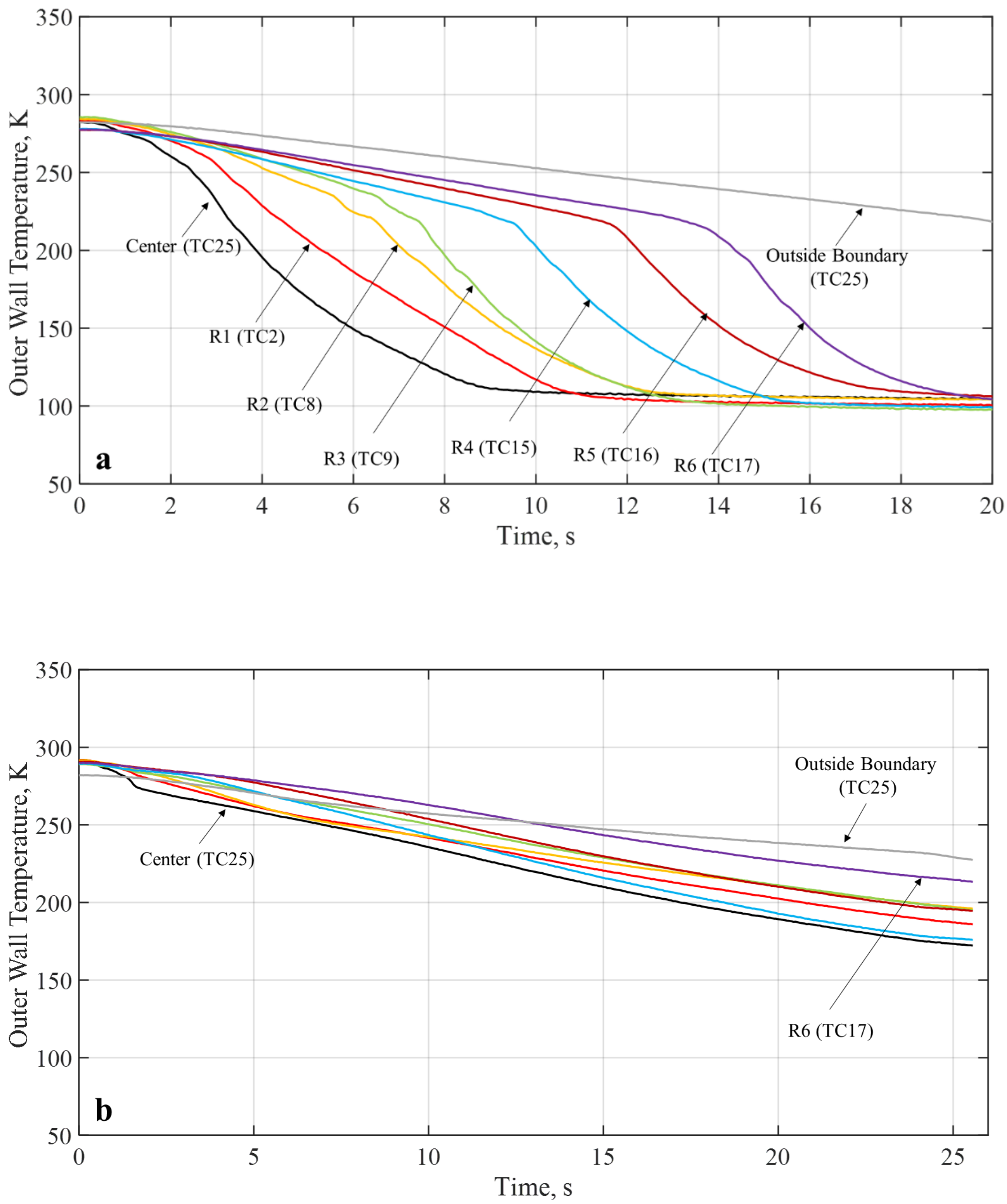

Fig. 7. Simplified chilldown curves for micro-G, 80 psig inlet pressure, 70% DC, 1s period (Case 3), (a) Teflon coated disk (b) stainless steel disk.

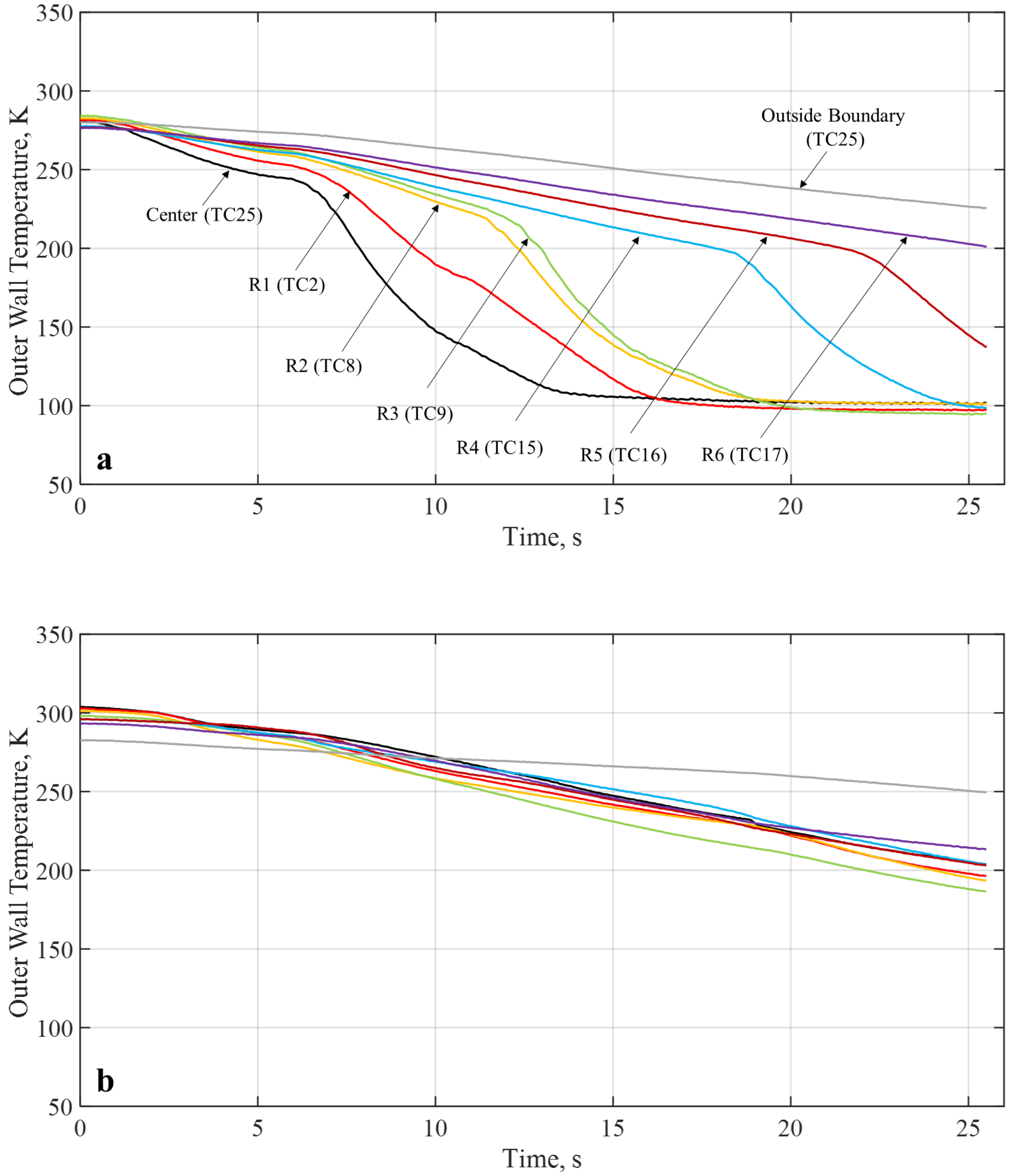

Fig. 8. Simplified chilldown curves for micro-G, 60 psig inlet pressure, continuous flow (Case 4), (a) Teflon coated disk (b) stainless steel disk.

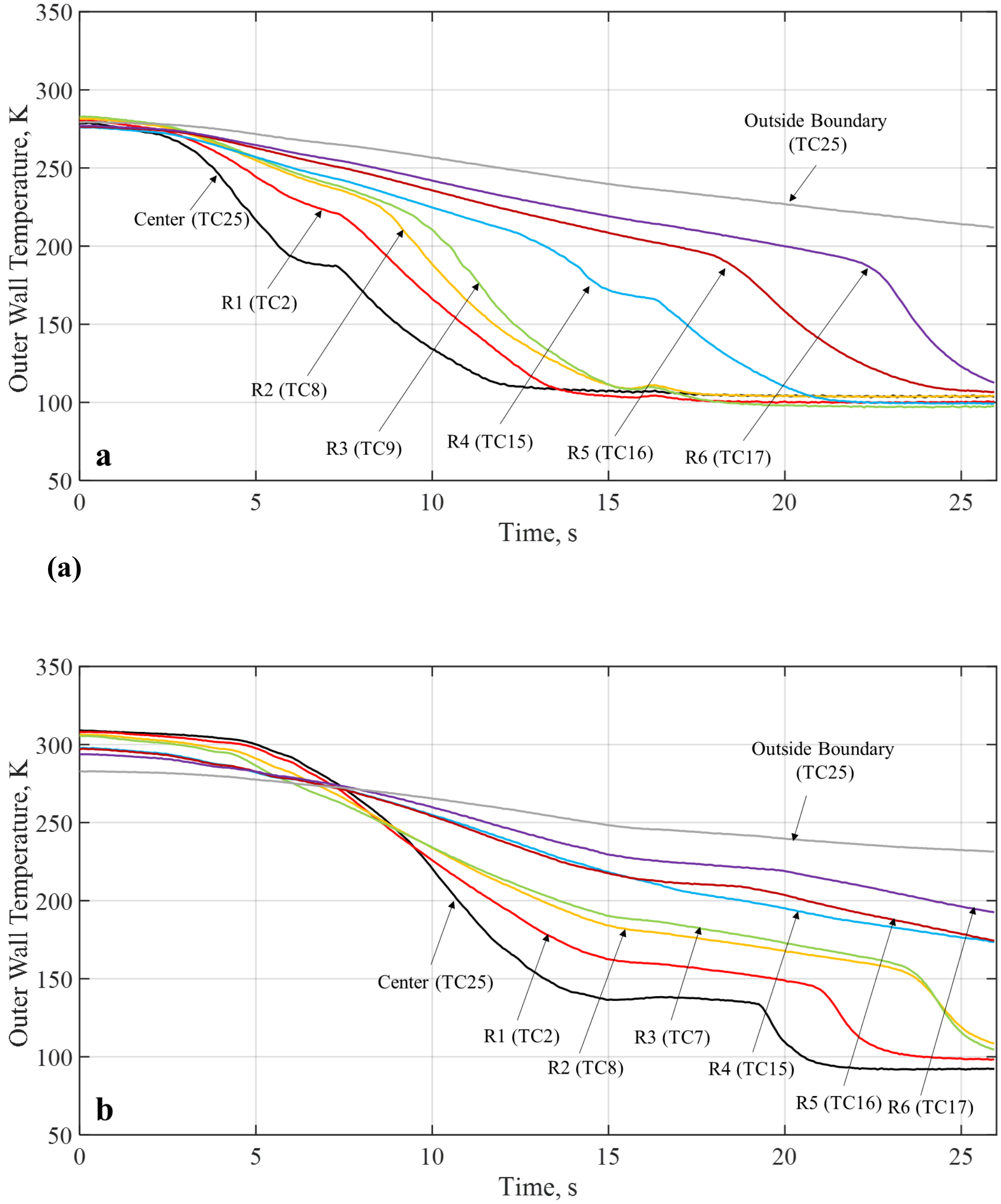

Fig. 9 Simplified chilldown curves for micro-G, 90 psig inlet pressure, continuous flow (Case 5), (a) Teflon coated disk (b) stainless steel disk.

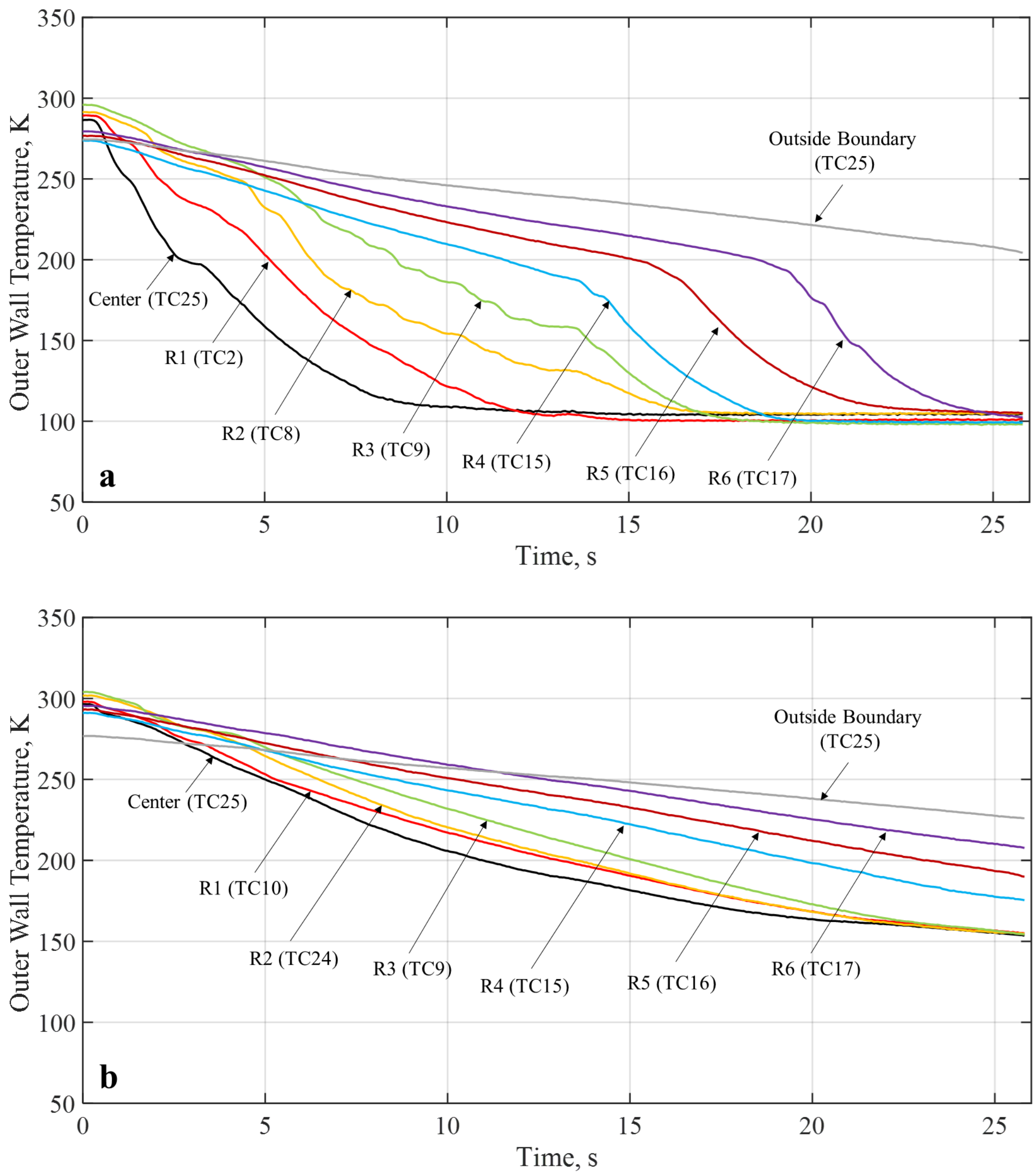

Fig. 10. Simplified chilldown curves for micro-G, 90 psig inlet pressure, 50% DC, 1s period (Case 6), (a)Teflon coated disk, (b) stainless steel disk.

Effects of gravity on disk chilldown heat transfer

Based on the spray chilldown data obtained in microgravity and terrestrial gravity, the effects of gravity on spray quenching are assessed in terms of the chilldown efficiency listed in Table 3. In general, for continuous flows, the gravity was found to enhance the chilldown efficiency for both coated and bare surface disks. The chilldown efficiencies in microgravity are 2% to 32% lower than those counterparts in terrestrial gravity for Cases 1, 4, and 5. The only exception is the coated disk in Case 4 where the efficiency is 16% higher in microgravity. However, the trend is somewhat mixed for pulse flows. For Case 2, the gravity almost made no difference. However, for Case 3, the efficiency is higher for coated tube and lower for bare surface disk in microgravity versus in terrestrial gravity. While for Case 6, the efficiencies are higher for both coated and bare surface disks in microgravity.

To explain the above, we offer the following. For the continuous flows, the higher efficiencies in terrestrial gravity are basically due to two heat transfer enhancement mechanisms. Natural convection that is induced by gravity is the first mechanism when the film boiling is taking place on the disk surface, while the draining and thinning of the liquid film during the transition and nucleate boiling would be the second mechanism that enhances the heat transfer. However, for the pulse flows we may not have the stable vapor films nor liquid films for heat transfer enhancement.

Effects of disk coating on chilldown heat transfer

In previous sections, we have already touched on some aspects of the low-thermal conductivity coating effects. Here, we would summarize those effects. Table 4 lists the percent increase in efficiency for the coated disk over the bare surface disk in both microgravity and terrestrial gravity. Consistently without any exception, the coating enhanced the heat transfer during spray chilldown as shown in Table 4 for all six cases in both microgravity and terrestrial gravity. However, for each case, the improvement in microgravity is always higher than that in terrestrial gravity that is basically due to the fact the efficiencies for bare surface disks are all lower in microgravity than those in terrestrial gravity as explained above. Therefore, there is more room for improvement. The results of coating effects thus confirm the theoretical basis for low-thermal conductivity coating given above.

Table 4. Improvement of chilldown efficiency by coating

	Reduced-G	Ground-G
Case	Percent Improvement	Percent Improvement
1 (micro-g) 80 psig, continuous flow	38.6%	18.7%
2 (micro-g) 80 psig 40% DC, 1s Period	34.1%	31.1%
3 (micro-g) 80 psig 70% DC, 1s Period	72.0%	19.1%

4 (micro-g) 60 psig, continuous flow	59.3%	31.9%
5 (micro-g) 90 psig, continuous flow	30.2%	20.5%
6 (micro-g) 90 psig 50% DC, 1s Period	28.2%	22.4%

Effects of flow pulsing on chilldown heat transfer

Let us first compare the efficiencies for Cases 1, 2, and 3 for the flow pulsing effects as they all have the same inlet pressures of 80 psig. As can be seen from Table 3 that for Case 2 pulse flow with 40% DC and 1s period, all four efficiencies are higher than the corresponding ones in Case 1 of continuous flow. Specifically, in microgravity, the improvements in efficiencies due to pulsing are 54% and 59% for coated and bare surface tubes, respectively. But for Case 3 with 70% DC and 1s period, the only pulse flow improvement over the continuous flow case is 27% for the coated disk in microgravity and the other three are either about the same (bare surface in microgravity) or less efficient (coated disk and bare surface disk in terrestrial gravity). Next, between Cases 5 and 6, all four efficiencies from the pulse flow Case 6 are higher than those corresponding ones with the continuous flow Case 5. Again, in microgravity, the improvements in efficiencies due to pulsing are 42% and 44% for coated and bare surface tubes, respectively. We may conclude that pulse flows can improve the chilldown the efficiency, but only with lower duty cycles.

Combined effects of disk coating and flow pulsing on chilldown heat transfer in microgravity

First let us compare between coated disk of Case 2 and bare surface disk of Case1 in microgravity. We found that the improvement due to both coating, and 40% DC and 1s period pulse flow is 113% for a common inlet pressure of 80 psig. The other comparison is between coated disk of Case 6 and bare surface disk of Case5 in microgravity. The improvement due to both coating, and 50% DC and 1s period pulse flow is 84% for a common inlet pressure of 90 psig.

Effects of inlet pressure on chilldown heat transfer

Cases 1, 4, and 5 provide information for assessing the inlet pressure effects. First, we need to stress that the mass flow rate is actually proportional to the inlet pressure as the flow is driven by the pressure difference between the inlet pressure and the pressure at the outlet. Since the outlet pressure is relatively constant that makes the mass flow rate to be totally dependent on the inlet pressure. As a result, it is the case that the higher the inlet pressure, the higher the mass flow rate. As explained above, the chilldown efficiency is inversely proportional to the mass flow rate that leads to the outcome that Case 4 should possess the highest efficiency, Case 1 is in the middle, and

Case 5 is the least efficient for each of the four categories (coated disk in microgravity, bare surface disk in microgravity, coated disk in 1-g, and bare surface disk in 1-g). It turned out that only the bare surface disk in 1-g did not follow the predicted trend, where Case 1 has the highest efficiency instead of Case 4 and Case 5 is still the lowest.

DISCUSSION

The experimental results obtained indicate a general trend that the enhancement on heat transfer and the improvement on the chilldown efficiency are mostly due to the low-thermal conductivity coating layer, especially in microgravity. An explanation is provided here. Based on the heat transfer physics and a theoretical analysis, there should exist an optimal thickness for the low-thermal conductivity coating layer that would give rise to the maximum chilldown efficiency. This optimal coating thickness would provide the most rapid cooling rate of the bulk disk material. The reason is that there are two heat transfer mechanisms involved that are opposite in nature to each other. The first mechanism is the thermal insulating effect due to the low-thermal conductivity thin layer that facilities a very quick drop of the disk surface temperature by restricting the heat flow from the bulk of the disk wall to the disk surface. This lower surface temperature allows the quenching process to move from film boiling regime to transition and nucleate boiling regimes in a much shorter time period, thus shortening the period of poor heat transfer film boiling regime. Also, the heat conduction theory predicts that the thicker the low-thermal conductivity layer, the quicker the surface temperature drops. The second mechanism is the conduction of heat from the bulk of the disk to the cooling fluid through the disk surface that requires the thickness of the coating material to be as thin as possible to expedite the wall cooling process. As a result, there should exist an optimal thickness of the low-thermal conductivity coating layer that balances these two competing mechanisms such that the coating is just thick enough to quickly lower the disk surface temperature to that of the Leidenfrost point while it is still relatively thin not to substantially reduce the heat flow from the bulk to the cooling fluid. Since we only had one flight, we were not able to test different coating thicknesses.

METHODS

Experimental system

Fig. 11 shows the photos of the parabolic flight experimental system. The test chamber of this apparatus is designed to comprise two nozzles to spray liquid nitrogen onto two separate stainless-steel circular disks simultaneously. All the system components except the high-pressure gas cylinder fit into a (L x W x H) 1.4m X 0.8m X 1m 8020 aluminum frame. This highly integrated thermal-fluid system was installed on the floor of ZERO-G Corporation’s Boeing 727-200F aircraft[21] to perform the parabolic flight disk chilldown experiment in a simulated reduced gravity environment. The reduced gravity is achieved through flying the aircraft in a parabolic trajectory and each parabola provides about 17-20 s reduced gravity (10^{-2}g) period.

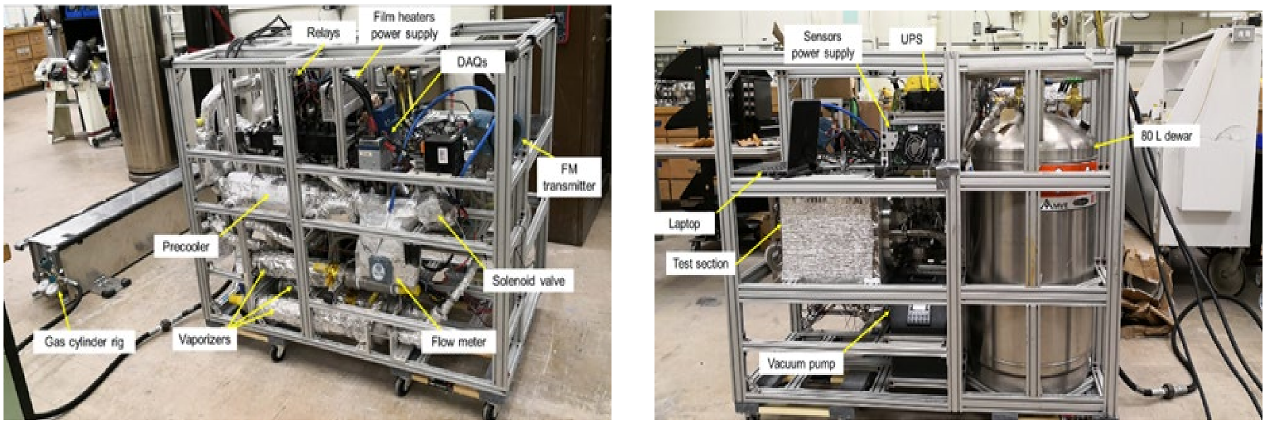

Fig. 11. Photographic images of the experimental system.

The experimental apparatus consists of four essential fluid units together with auxiliary components, fluid piping and instrumentations. The fluid piping schematic and instrumentation diagram is shown in Fig. 12. The 80 L double-wall cryogenic dewar supplies the LN2 to the test section for performing the disk chilldown test as well as provides the LN2 for the pre-chilling of all the fluid components upstream of the test section prior to the actual chilldown test. Before the experiment, the 80 L dewar is topped off with industrial grade liquid nitrogen from a standard Airgas 180-Liter dewar through the LN2 fill port. The subcooler is essentially a simple shell-tube heat exchanger (Fig. 13) and it serves two functions. The first one is to subcool the liquid nitrogen before it enters the test section such that the thermodynamic state of the liquid entering the test section can be determined. During the subcooler operation, the inner finned tube of the subcooler is totally submerged in the liquid nitrogen bath on the shell-side. Since the pressure inside the tube is always higher than that on the shell side, the liquid nitrogen bath is always colder than that inside the tube. Thus, heat is removed from the liquid in the tube side. The second function is to save the liquid nitrogen during the pre-test chilldown of the upstream components of the test section. The vapor generated on the shell side is separated by gravity and is vented outside the system.

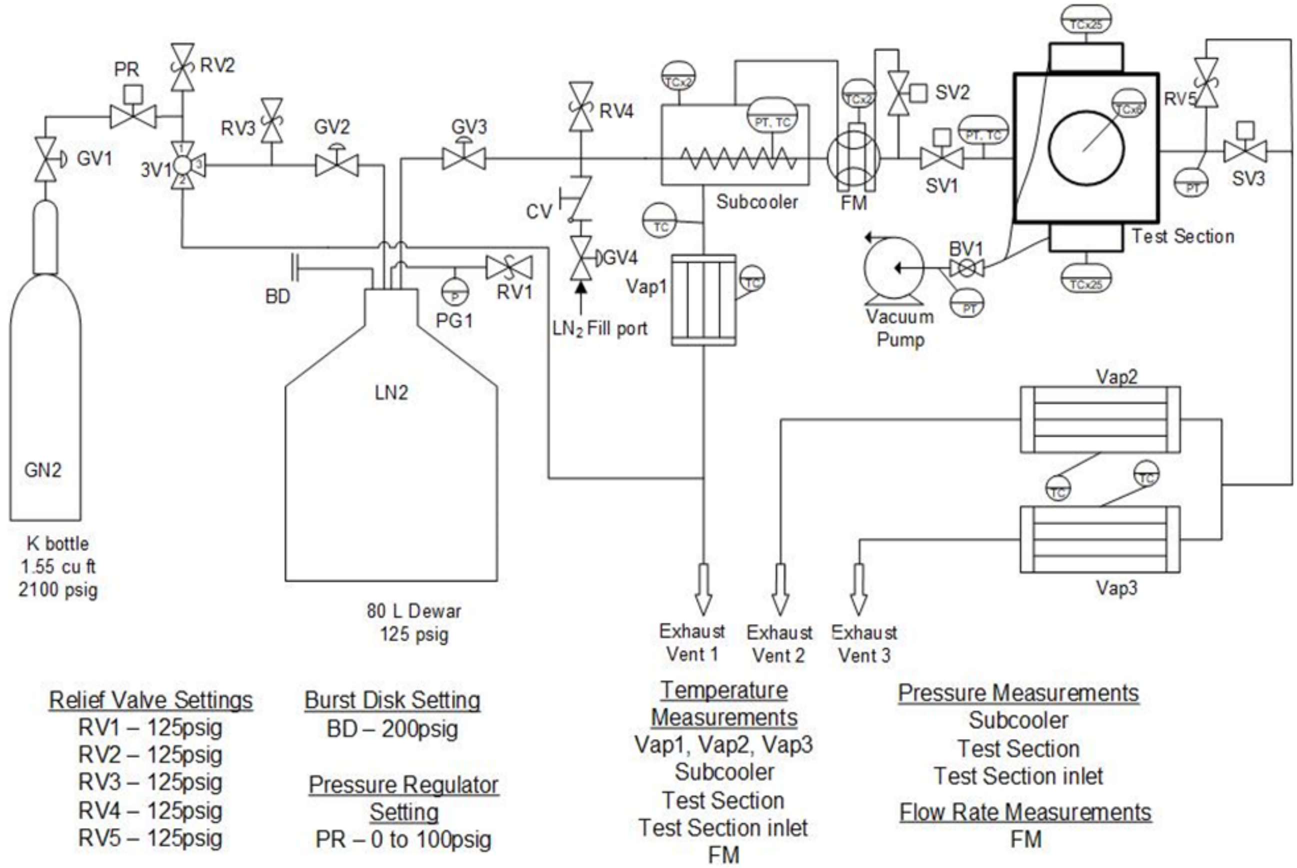

Fig. 12. Fluid system schematic. The valves and important components of the fluid network. Relief valve settings, the burst disk setting, and pressure regulator settings are also included. BD, burst disk; BV, ball valve; CV, check valve; FM, flow meter; GN2, gaseous nitrogen; GV, globe valve; LN2, liquid nitrogen; PG, pressure gauge; PR, pressure regulator; PT, pressure transducer; RV, relief valve; SV, solenoid valve; TC, thermocouple; Vap, vaporizer; 3V, three-way valve.

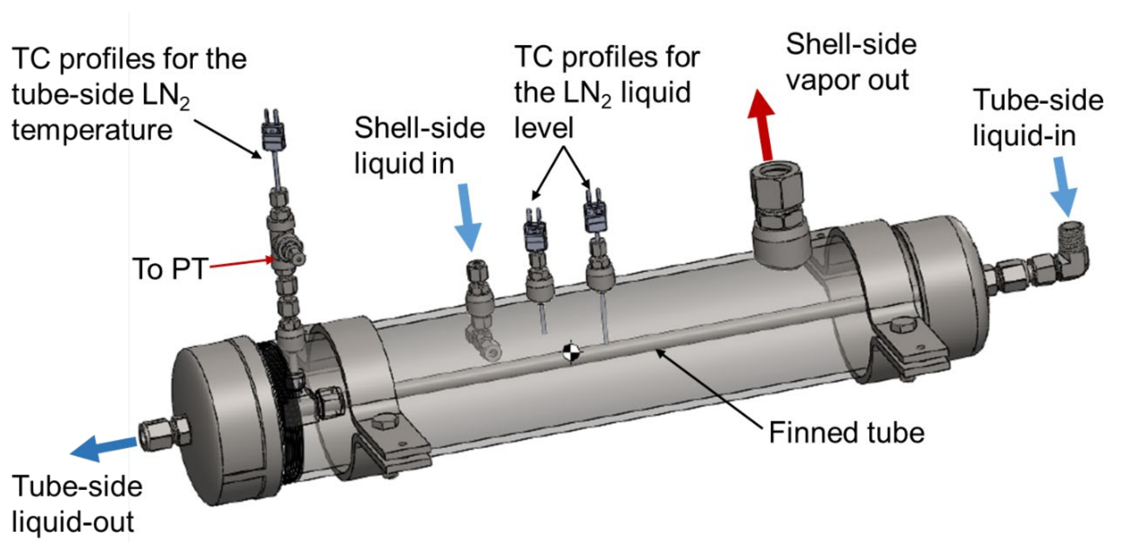

Fig. 13. A CAD drawing of the subcooler.

The test section is basically a vacuum chamber where the cryogenic spray cooling of the disk takes place during the experiment and it is made mostly by off-the-shelf vacuum components. The exploded view of the test section is given in Fig. 14, which shows the configuration of the two test disks and two spray nozzles. Two spray nozzles are placed at the center between two disks inside the 10-inch cubic vacuum chamber. Two stainless steel disks, cut from a 16-gauge 304 stainless steel sheet with a thickness of 0.058 inch, were mounted at opposite sides of the chamber, for example, the front and back or top and bottom. Depends on the purpose of the test, either one set of nozzle and plate or two sets of nozzles and plates are installed. For the ground test, only the single nozzle and one plate were installed inside the test chamber. The orientation of the heat transfer disk surface with respect to the gravity direction is varied by placing the stainless-steel disk at the bottom, side, or top of the cubic test chamber, and they are referred as upward, vertical, and downward configurations. For the flight tests, two different disk plates and two nozzles were installed as show in Fig. 14. Each disk is sandwiched by two bored vacuum flanges. Two PTFE gaskets were compressed against the stainless-steel disk such that the cubic test chamber and the back of the disk can be sealed. The outermost flange on each test disk assembly is connected to the vacuum pump such that the back of the stainless-steel disk is insulated from the surroundings by drawing vacuum to minimize the parasitic heat input from the outside environment. For measuring the disk transient temperature history during the chilldown, 25 thermocouples (TCs) were soldered to the vacuum side (back) of each stainless steel disc. As shown in Fig. 15, a total of 24 TCs were distributed on the 7 concentric circles (7 rings, R1, R2,…,R7) in addition to one (TC25) placed at the center. Only one TC (TC5) is placed on the outermost ring, R7, near the outer boundary. TC5 is 3.7" away from the center of the plate. Eight MINCO film heaters (Hap 6945 and 6946) are attached to the back of the disk to reheat the stainless steel plate back to the initial temperature for the next test after each chilldown test.

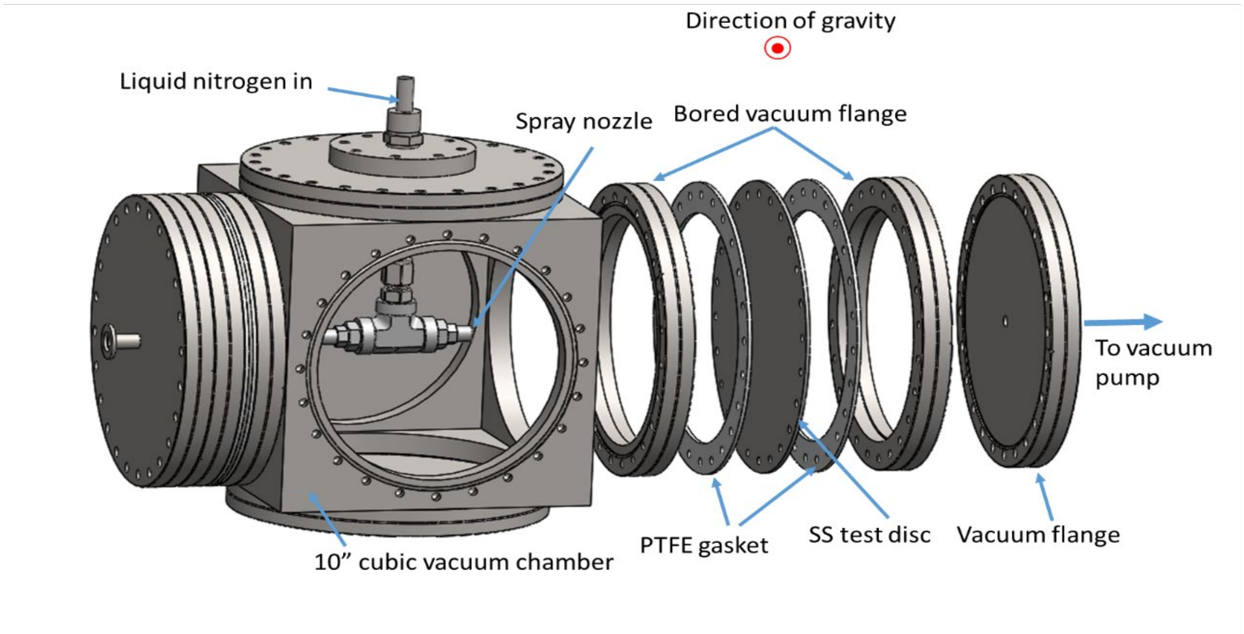

Fig. 14. A CAD drawing of the test section.

The flow coming out of the test section goes into two separate vaporizers in parallel (labeled as Vap2 and Vap3 in Fig. 12). The vaporizers are basically heat exchangers made from tube bundles, which evaporate any remaining liquid nitrogen coming out of the test section and also heat up the cold nitrogen vapor to above 0 °C before venting pure vapor out of the system. Each vaporizer is made by packing eight grooved copper tubes that have star shaped inner insertions into a 2.5" schedule 40 stainless steel pipe. The tube bundles are heated up to 200 °C before each test by a high temperature heating tap that is wrapped around the outer surface of the stainless steel pipe. The Labview program monitors and controls the on and off of the heating tap by the combination of K type thermocouple, NI 9211 thermocouple input module, NI 9472 digital output module, and a mechanical relay. If the experiment is performed on board the aircraft, the gas coming out of the vaporizers is vented outside the aircraft cabin through rubber hoses that connect to the vent ports on the cabin wall. Similarly, another vaporizer, Vap1 ensures the proper venting of gaseous nitrogen coming out of the subcooler.

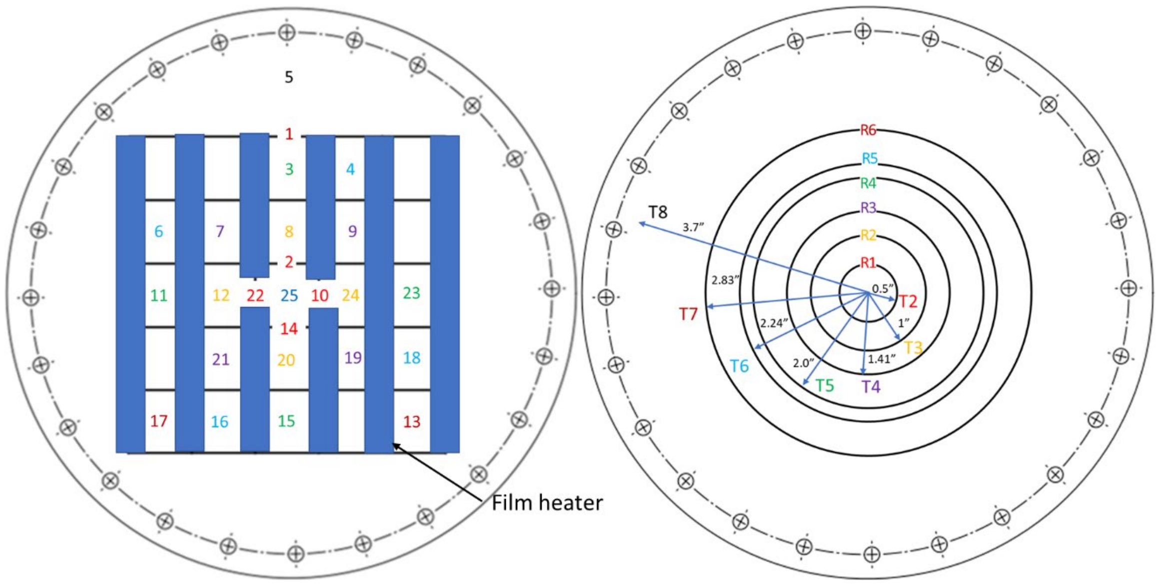

Fig. 15. A schematic showing the layout of thermal couples.

The data acquisition system including Labview program and National Instrument Compact DAQ hardware collects all sensor data and displays them real time on a laptop at a sampling rate of 16 Hz. NI 9214 TC modules read all the T-type TCs (Omega). NI 9205, an analog input module, reads all the voltage signals from pressure transducers (Omega PX 409V5A) and the 4-20 mA current signals (through a 249 ohm resistor) from the Coriolis liquid flow meter (Micro motion CMF025). The Labview program controls the opening and closing of the solenoidal valve, SV1, through a combination of NI USB 6009 and Solid-State relay. In the case of continuous spray, the relay energizes the solenoid valve after receiving a continuous voltage signal. However, in the case of intermittent spray, the relay energizes and de-energizes SV1 according to a rectangular waveform voltage signal from the VI.

In the current experiment, we used two types of disks. In addition to the bare surface stainless steel disk, we also added a coated disk that is a stainless-steel disk coated with a low-thermal conductivity thin-film Teflon layer on one side of the disk surface. Specifically, the coating material was made of Fluorinated Ethylene Propylene (FEP) by DuPont and classified by DuPont as Teflon 959G-203 that is a black color paint and has a thermal conductivity of 0.195 W/mK (DuPont publication[22]). The coating was put on using the dip and drain process. The thickness of the coating is estimated at around 20-30 microns.

Experimental procedure

To perform the chilldown test, mainly four steps are followed, and these are initial starting, pre-cooling, testing, and reheating. The initial starting is the step where all the electrical devices are turned on. This includes running the pre-programed Labview script and turning on the vacuum pump (Turbo Lab 80). Once the Labview script is running, it will automatically set the output voltage of the DC power supply for the pressure transducers and turn on the heating cables of the vaporizers. This step takes about 30 minutes mainly due to the time required for heating up the vaporizers to 200 °C. Meanwhile, the globe valves, GV1, GV2, GV3 are open for the next step. The second step involves the pre-cooling and pre-chilling of all the piping and fluid components upstream of the test section to make that only liquid phase of working fluid to enter the test section and it proceeds first by rotating the three-way valve, 3V1, from GV1 to GV2, and setting the desired testing pressure on the pressure regulator, PR. Once the solenoidal valve SV2 is open by clicking the virtual button on the Laptop screen, then the liquid nitrogen starts to flow from the 80 L dewar into the shell-side of the subcooler. Before the liquid nitrogen can fill up the shell-side of the subcooler, the flow path upstream of the test section has to be chilled down. This step prevents the boil-off of liquid nitrogen before it flows into the test section. Once the inner tube of the subcooler is full (can be determined by the profile reading of the TC located inside the subcooler), the system is ready for the experiment. The chilldown test is started simply by clicking the virtual start bottom on the laptop screen, then the solenoid valve, SV1, will be opened according to the preset waveform signals either to continuously or intermittently flow nitrogen into the test section for spraying on the target disks. Once all the temperature readings from the TCs drop to the liquid nitrogen temperature and maintain at a steady state, the disk chilldown experiment is complete. The solenoid valve, SV1, is then closed by clicking the virtual stop bottom. Next, the reheating step starts to prepare the stainless steel disc plates for the next test. To heat up the plates after chilldown, the film heaters are turned on by clicking the heating virtual bottom on the screen. Once the plates are heated back to the room temperature, the film heaters are turned off. This marks the beginning of the next cycle of testing which starts with the pre-cooling step.

In addition to the experimental procedure discussed above, next we need to mention the simulated microgravity environment on the parabolic flight. The variable gravity condition inside the airplane was created when the airplane is flying a parabolic trajectory. Fig. 16 provides the information on the parabolic flight gravity-level versus time characteristics[21]. The microgravity period is always sandwiched by two 1.8-g periods where g is the earth gravity of 9.81 m/s^2. The microgravity period nominally lasts between 18-25 seconds. For our research flights, in order to maintain the acceleration levels within ±0.01g, the microgravity period is around 18-20 seconds.

Experimental uncertainty

Table 5 lists all the uncertainties or the independently measured quantities. The uncertainty for the chilldown thermal efficiency is discussed above in the Results section.

Table 5. Measured quantities and uncertainties

Symbol	Quantity	Measurement method	Uncertainty
T	Plate temperature	T-type thermocouple	1 K or 1.5% below 273 K
P_c	Test section pressure	Kulite CTL-190M140BARA	7 kPa
δ	SS plate thickness	Calipers	0.03 mm

R_x	Radial position of TCs on Ring x	Ruler	1.6 mm (1/16")
$\dot{m}$	LN_2 mass flow rate	Coriolis flow meter	0.3%
M	Mass of the fluid components (tube, tee, nozzle)	scale	0.1 g

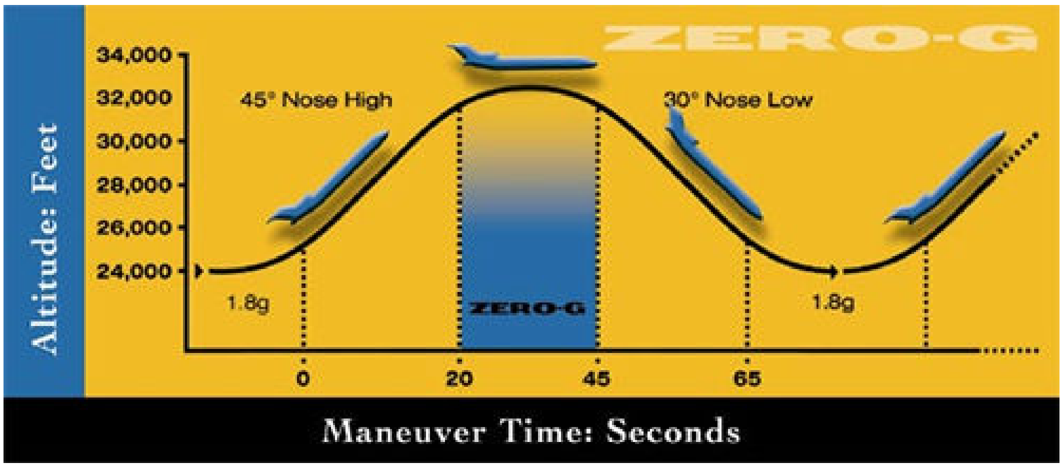

Fig. 16. Schematic of parabolic flight variable gravity levels vs. time

Reporting summary

Further information on research design is available in the Nature Research Reporting Summary linked to this article.

DATA AVAILABILITY

The authors declare that the data supporting the findings of this study are available within the paper.

REFERENCES

1. Mars Architecture Steering Group. Human exploration of Mars Design Reference Architecture 5.0. Report No. NASA/SP-2009-566 (ed. Drake, B. G.) (National Aeronautics and Space Administration) (2009).
2. Meyer, M. L. et al. Mastering cryogenic propellants. J. Aerosp. Eng. 26, 343–351 (2013).
3. Motil, S. M., Meyer, M. L. & Tucker, S. P. Cryogenic fluid management technologies for advanced green propulsion systems. AIAA 45th Aerospace Sciences Meeting and Exhibit; NASA/TM-2007-214810, Reno, NV, 8 January (American Institute of Aeronautics and Astronautics, 2007).
4. NASA. NASA Technology Roadmaps, TA 2: In-Space Propulsion Technologies (National Aeronautics and Space Administration, 2015).
5. Shaeffer, R., Hu, H. & Chung, J. N. An experimental study on liquid nitrogen pipe chilldown and heat transfer with pulse flows. Int. J. Heat Mass Transf. 67, 955–966 (2013).
6. Doherty, M.P. Gaby, J.D., Salerno, L.J. & Sutherlin, S.G. "Cryogenic Fluid Management Technology for Moon and Mars Missions", **NASA/TM—2010-216070, also published as AIAA–2009–6532**.

7. Meyer, M.L., Chato, D.J., Plachta, D.W., Zimmerli, G.A., Barsi, S.J., Van Dresar, N.T. & Moder, J.P. "Mastering Cryogenic Propellants", ***JOURNAL OF AEROSPACE ENGINEERING***, APRIL 2013, pp. 343-351.
8. Liang, G. & Mudawar, I. Review of spray cooling – Part 1: Single-phase and nucleate boiling regimes, and critical heat flux, Int. J. heat Mass Trans. 115 (2017) 1174-1205.
9. Carey, V. P., Liquid-Vapor Phase-Change Phenomena. 2nd edn (Taylor & Francis Group, LLC., 2008).
10. Liang, G. & Mudawar, I. Review of spray cooling – Part 2: High temperature boiling regimes and quenching applications, Int. J. heat Mass Trans. 115 (2017) 1206-1222.
11. Sehmbey, M.S. Chow, L.C., Hahn, O.J. & Pais, M.R. Spray cooling of power electronics at cryogenic temperatures, J. Thermophysics Heat Trans. 9 (1995) 124-128.
12. Sehmbey, M.S. Chow, L.C., Hahn, O.J. & Pais, M.R. Effect of spray characteristics on spray cooling with liquid nitrogen, J. Thermophysics Heat Trans. 9 (1995) 757-765.
13. Somasundaram, S. & Tay, A. "Comparative study of intermittent spray cooling in single and two phase regimes," *International Journal of Thermal Sciences,* vol. 74, pp. 174-182, 2013. DOI: https://doi.org/10.1016/j.ijthermalsci.2013.06.008.
14. Kato, M. *et al*, "Spray cooling characteristics under reduced gravity," *J. Thermophys. Heat Transfer,* vol. 9, *(2),* pp. 378-381, 1995. Available: https://doi.org/10.2514/3.675. DOI: 10.2514/3.675.
15. Yoshida, K. *et al*, "Spray cooling under reduced gravity condition," *Journal of Heat Transfer,* vol. 123, *(2),* pp. 309-318, 2001.
16. Bergman, T. L. et al. Fundamentals of Heat and Mass Transfer, 7th edn (Wiley, 2011).
17. Chung, J. N., Darr, S. R., Dong, J. & Wang, H. Enhancement of convective quenching heat transfer by coated tubes and intermittent cryogenic pulse flows. Int. J. Heat Mass Transf. 141, 256–264 (2019).
18. Chung, J. N., Darr, S. R., Dong, J., Wang, H. & Hartwig, J. W. Heat transfer enhancement in cryogenic quenching process. Int. J. Therm. Sci. 147, 106117(2020). Article Number.
19. Chung, J. N., Darr, S. R., Dong, J., Wang, H. & Hartwig, J. W. An advance in transfer line chilldown heat transfer of cryogenic propellants in microgravity using microfilm coating for enabling deep space exploration. npj Microgravity (2021) 7:21 ; https://doi.org/10.1038/s41526-021-00149-5.
20. Burggraf, O. R. An exact solution of the inverse problem in heat conduction theory and applications. J. Heat Transf. 86, 373–380 (1964).
21. Zero-g Corporation, https://www.incredible-adventures.com/zero-g-how.html
22. DuPontTM Teflon FEP, Fluoroplastic Film (2013), WWW.teflon.com/Industrial.

ACKNOWLEDGEMENTS

A great amount of recognition is due to Peter Torsone, Noah Yudwitz, and Ben Frohn who helped carry out the parabolic flight experiments both as flyers and as ground support personnel. We are particularly grateful for the support and consultation provided by the Zero Gravity Corporation. This work was supported by the Flight Opportunities Program at National Aeronautics and Space Administration (NASA) under the award number 80NSSC18K0367. This research was also partially supported by the Andrew H. Hines, Jr./Progress Energy Professorship Endowment Fund at the University of Florida and the Department of Mechanical and Aerospace Engineering at the University of Florida.

COMPETING INTERESTS
The authors declare no competing interests.

AUTHOR CONRIBUTION

J.N.C. was the principal investigator, conceived the concept, and performed the literature review, analysis, and manuscript preparation. J.D. was the lead experimenter who designed the experimental system and built the apparatus, completed some of the data reduction and analysis. H.W. performed some experiment, data reduction, analysis and manuscript preparation, including many of the plots and figures. S.R.D. contributed towards the experiment design, experimentation, and data discussion. J.W.H. assisted in the experiment design, experimentation, and general discussion.